LAWRENCE
LIVERMORE
NATIONAL
LABORATORY

LLNL-CONF-855676

Recent Progress of Plasma Exhaust Concepts and Divertor Designs for Tokamak DEMO Reactors

N. Asakura, K. Hoshino, S. Kakudate, F. Subba, J. H. You, S. Weisen, T. D. Rognlien, R. Ding, S. Kwon

October 9, 2023

25th International Conference on Plasma Surface Interaction in Controlled Fusion Devices
Jeju, Japan
June 12, 2022 through June 17, 2022

Disclaimer

LLNL-CONF-855676

Recent Progress of Plasma Exhaust Concepts and Divertor Designs for Tokamak DEMO Reactors

N. Asakura[1], K. Hoshino[2], S. Kakudate[1], F. Subba[3], J.-H. You[4], S. Weisen[5], T.D. Rognlien[6], R. Ding[7], S. Kwon[8]

[1] *National Institutes for Quantum Science and Technology (QST), Naka, Ibaraki 311-0193 Japan*

[2] *Graduate School of Science and Technology, Keio University, Yokohama 223-8522, Japan*

[3] *NEMO Group, Politecnico di Torino, Torino, Italy*

[4] *Max Planck Institute for Plasma Physics, Boltzmannstrasse 2, Garching, Germany*

[5] *Forschungszentrum Jülich GmbH, Institut für Energie und Klimaforschung Plasmaphysik, 52425 Jülich, Germany*

[6] *Lawrence Livermore National Laboratory, Livermore, CA, 94551, USA*

[7] *Institute of Plasma Physics, Chinese Academy of Sciences, Hefei 230031, China*

[8] *National Fusion Research Institute, Daejeon 34133, Republic of Korea*

ABSTRACT

Power exhaust concept and appropriate divertor design are common critical issues for DEMO design activities, which have been carried out in Europe, Japan, China, Korea and USA. Conventional divertor concepts and power exhaust studies for recent DEMO designs (P_{fusion} = 1-2 GW, R_p = 7-9 m) were reviewed from the viewpoints of the plasma physics study and the divertor engineering design. Radiative cooling is a common approach for the power exhaust scenario. Requirements of the main plasma radiation fraction ($f_{rad}^{main} = P_{rad}^{main}/P_{heat}$) and the plasma performance determine the divertor design concept. Different challenges, (i) increasing the main plasma radiation fraction and simplifying the divertor geometry for ITER-level P_{sep}/R_p design, and (ii) extending ITER divertor geometry with increasing divertor radiation (P_{rad}^{div})

for larger $P_{sep}/R_p \geq 25 MWm^{-1}$ design, will contribute to optimize the future DEMO design. ITER-based divertor geometry with longer leg length (1.6-1.7 m) is a common baseline design, and power exhaust simulations with larger P_{sep} =150-300 MW have been performed using integrated divertor codes. Geometry effects (ITER like one or more open one without baffle) on plasma detachment profile and the required divertor radiation fraction ($f_{rad}^{div} = P_{rad}^{div}/P_{sep}$) were important key. All simulations showed reduction in the peak $q_{target} \leq 10 MWm^{-2}$ for the large f_{rad}^{div} = 0.7-0.8, while the peak q_{target} location and value were significantly different in the partial detached divertor. Simulation results also demonstrated that diffusion coefficients of heat and particle fluxes were a critical for DEMO divertor design, and that effects of various drifts on outboard-enhanced asymmetry of the heat flux, which may need further longer led to insure the detached divertor operation window.

Integrated design of the water cooled divertor target, cassette body (CB) and cooling pipe routing has been developed for each DEMO concept, based on the ITER-like tungsten monoblock (MB) and Cu-alloy pipe. Engineering design adequate under higher neutron irradiation condition was required. Therefore, inlet-T_{cool} was increased and has so far large variation between 70 ℃ and 200 ℃. Influence of thermal softening on the CuCrZr pipe was fostered near the strike-point when the high q_{target} of 10 MWm^{-2}-level was exposed. Improved technologies of high heat flux components based on the ITER W-MB unit have been developed in EU. Two coolant conditions (lower- and higher-T_{cool}) and routes for the Cu-alloy and RAFM steel heat sink MB units, respectively, and the latter coolant was also provided for CB and supporting structures. Appropriate conditions for the latter coolant, i.e. 180°C/ 5 MPa (EU-DEMO) and 290°C/ 15 MPa (JA DEMO, CFETR and K-DEMO), will be determined in the future optimization of the divertor and DEMO design.

Corresponding Author Address:
Plasma Theory and Simulation Group, Naka Fusion Institute, QST
801-1 Mukoyama, Naka, Ibaraki-ken 311-0193 JAPAN
Corresponding Author e-mail: asakura.nobuyuki@qst.go.jp
Presenting author: Nobuyuki Asakura
Corresponding Author Tel: +81-29-270-7263
Keywords: DEMO, Power exhaust, Divertor simulation, Divertor design, Water-cooling divertor

1. Introduction

Demonstration of electricity production larger than internal consumption is the most outstanding challenge of DEMO fusion reactor. The fusion power (P_{fusion}) and device size (major radius: R_p) are increased in order to achieve electricity generation larger than the internal consumption (net electricity generation), and tritium breading sustainable for the fusion reaction (self-sufficient tritium breading). Power exhaust concept and the appropriate divertor design are common critical issues for DEMO design activities, which have been carries out in Europe, Japan, China, Korea and USA. Representative plasma parameters and heating power of recent DEMO concepts [1-8] are investigated by using tokamak system codes as shown in Table 1. Those for ITER [9,10] are added. EU DEMO1 baseline design (R_p/a_p = 9.0/2.9 m, a_p: midplane minor radius) is shown. Power handling concept of a recent proposal, i.e. Flexi-DEMO [11] (R_p/a_p = 8.4/2.71 m, aiming for not only a pulsed operation but also a steady-state operation if the plasma performance is improved), is similar to the baseline design. Pulsed operation performance was also investigated in the steady-state design of JA DEMO 2014 (R_p/a_p = 8.5/2.4 m) [3]. For CFETR (R_p/a_p = 7.2/2.2 m) [5] and K-DEMO (R_p/a_p = 6.8/2.2 m) [6,7], plasma parameters at the first stage are shown. Design activity for FNSF (R_p/a_p = 4.8/1.2 m) [8] was recently reviewed, which aims developing sufficient engineering and technology for tritium breading (TBR ~1.0) and electricity production (equal to internal consumption). A power plant concept ARIES-ACT1 [12] (R_p/a_p = 6.25/1.56m) will achieve above DEMO missions in USA.

Generally, pulse DEMO concept has larger P_{fusion}, and steady-state concepts require to increase auxiliary power (P_{aux}) for current drive of the plasma current (I_p). The total heating power (P_{heat}) by α-particles (P_α) and P_{aux} of these DEMO concepts is increased to 1.8-3 times larger than that of ITER, while R_p is restricted from comparable to 1.5 times larger. A power exhaust parameter of P_{heat}/R_p (39-62 MWm^{-1}) suggests significant increase of the heat flux in the scrape-off layer (SOL), comparing to that of ITER (24 MWm^{-1}), without considering radiation loss in the main plasma (P_{rad}^{main}). Double null divertor design is proposed (K-DEMO, FNSF) or considered (EU DEMO1) for devices with P_{heat}/R_p larger than double of ITER. The power exhaust scenarios in the main plasma and divertor have been investigated for these DEMO concepts, where the radiative cooling by impurity seeding is a common approach. The total radiation fraction in the main plasma and divertor becomes large ($f_{rad}^{tot} = P_{rad}^{tot}/P_{heat} \geq 0.8$, where $P_{rad}^{tot} = P_{rad}^{main} + P_{rad}^{sol} + P_{rad}^{div}$: total radiation loss in the main plasma, SOL and divertor), compared to that for ITER (f_{rad}^{tot} = 0.6-0.7) in order to reduce the peak heat load on the divertor

target (q_{target}) to 10 MWm^{-2} level [9,10].

Conventional divertor designs were developed for these DEMO concepts, based on the ITER divertor. Power exhaust simulations in the divertor have been performed by integrated divertor simulation codes to predict a self-consistent transport solution of the plasma, neutral and impurities in SOL and divertor. Particularly for the reactor design, the plasma detachment is required to significantly reduce both the plasma ion and electron temperatures near the strike-points (T_i^{div}, T_e^{div}) and the peak q_{target}. Formation of the plasma detachment and the operation window under key power exhaust parameters such as exhaust power to the SOL ($P_{sep} = P_{heat} - P_{rad}^{main}$), radiation loss fraction in the SOL and divertor normalized by P_{sep} ($f^*_{rad}{}^{div} = (P_{rad}^{sol} + P_{rad}^{div})/P_{sep}$) and characteristic length of the heat flux profile in SOL (λ_q^{SOL}) have been investigated to determine appropriate divertor design [13-23]. Larger $f^*_{rad}{}^{div}$ is required with increasing the divertor power handling parameter (P_{sep}/R_p), compared to ITER ($f^*_{rad}{}^{div}$ = 0.5–0.6, P_{sep}/R_p = 16 MWm^{-1}) [24].

It is also necessary to develop the foreseeable technical solution of the divertor under severe neutron irradiation condition, compared to ITER. The design of the plasma facing components (PFCs) is mostly based on the ITER technology [25], i.e. tungsten (W) monoblock and cupper (Cu) alloy pipe for the heat sink of the water cooling concept. Here, helium (He) cooling concept is considered for FNSF and an option of EU DEMO1. Double null design will significantly affect engineering issues such as reinforcing the upper divertor coil, reducing tritium breeding blanket (BB) volume, and restricting the remote maintenance. In addition, accurate control of the double null plasma configuration to obtain the equal up-down power distribution is required, and outboard enhanced heat flux asymmetry in the SOL is also considered as a physics issue.

This paper reviews recent progress of the baseline power exhaust scenario of representative DEMO concepts and divertor design studies in order to identify critical issues and technical challenges in physics, engineering and technology. Common view and differences in the divertor design concepts are summarized. Power exhaust concepts for DEMO plasma designs are shown in Sec. 2. Section 3 reviews recent progresses of power exhaust simulations for DEMO divertor design; simulation codes and input conditions, plasma detachment and divertor operation, divertor geometry, W erosion estimation in the partially detached divertor, and effects of diffusion coefficients, are summarized. Concepts of the heat removal technology and the divertor engineering design, and their issues are summarized in Sec. 4. Progresses and key issues are summarized in Sec. 5. Advanced magnetic configurations and alternative concepts, transient heat load and PWI for DEMO are not covered.

2. Power exhaust concepts with impurity seeding

Power handling in the main plasma is determined by conflicting requirements of increasing the radiation loss fraction ($f_{rad}^{main} = P_{rad}^{main}/P_{heat}$) and the plasma performance as characterized by the enhancement factor of the energy confinement ($HH_{98(y,2)}$) and the normalized β (β_N). Power exhaust concepts were investigated in EU DEMO1 [1, 26] and JA DEMO higher plasma elongation (κ_{95} = 1.75: elongation at 95% of a_p) [27] from the parameter scans by EU and JA system codes (PROCESS [28] and TPC [29], respectively). Key power exhaust parameters for single null divertor DEMOs are summarized in Table 2. Different power exhaust scenarios were proposed for the EU and JA DEMO concepts.

EU DEMO1 aims for 2-hours pulse operation with producing net-electricity of P_{net} = 500 MW with P_{fusion} ~2 GW, which is based on the performance of ITER with conservative improvements in physics and technology. Design points of the DEMO size (R_p) and the toroidal field (B_T) were predicted as a function of P_{sep} ratio above the L to H-mode transition threshold power [30] ($f_{LH} = P_{sep}/P_{LH}$), with achieving ITER-level $HH_{98(y,2)}$ (1.1) and stable β_N (2.6) by impurity seeding as shown in Fig. 1(a)(b) [31]. Reference values for the divertor operation boundaries are shown by three thick lines; (i) maximum tolerable heat load condition of $P_{sep}B_T/q_{95}R_pA$ ~9 MWTm^{-1} (q_{95}: safety factor at 95% of a_p, $A = R_p/a_p$: plasma aspect ratio), (ii) critical impurity concentration in SOL to produce the divertor detachment ($c_{Z,det}$) comparable to a reference value (c_{REF}), which is consistent with the fuel dilution in the main plasma, and (iii) $P_{sep} = P_{LH}$. Here, $\hat{c}_{Z,det}$ is normalized value of $c_{Z,det}$ at f_{LH} = 1.38. Appropriate design points for the divertor operation ($P_{sep}B_t/q_{95}R_pA \leq 9$ MWTm^{-1}) and impurity concentration ($\hat{c}_{Z,det} \leq 1$) are shown within colored area (A and B), and EU DEMO1 design point (R_p = 9.0 m, B_T = 6 T) was determined at f_{LH} = 1.2 and existing superconductor technology ("A").

Therefore, the DEMO1 concept challenges increasing f_{rad}^{main} to ~0.67 by impurity seeding scenario with higher-Z impurities such as Kr and Xe, in addition to Ar in order to employ ITER-level power handling in the divertor (P_{sep}/R_p ~17MWm^{-1}), as shown in Fig. 2. Power exhaust parameters of Flexi-DEMO, i.e. f_{rad}^{main}~0.67 and P_{sep}/R_p ~20MWm^{-1} for the pulsed plasma and f_{rad}^{main}~0.61 and P_{sep}/R_p ~23MWm^{-1} for the steady-state plasma, are also added. It is noted that the ambiguity of P_{LH} is relatively small from the power threshold database in low Z_{eff} less than 2 [30], which will be applied to the ITER operation. Thus, further improvement of the database with regard to impurity seeding and P_{LH} scaling for higher Z_{eff} are necessary to determine P_{LH} for the DEMO plasma design. At the same time, another challenge of reducing the divertor

coverage, i.e. removing the divertor baffle, is proposed to increase the tritium BB volume. Such high f_{rad}^{main} was reported in the ASDEX-Upgrade (AUG) H-mode experiment with Ar and nitrogen (N) seeding [32, 33], and some representative database are plotted in Fig. 2.

JA DEMO aims for the steady-state operation with producing P_{net} of a few 100 MW with P_{fusion} ~1.5 GW and installing enough central solenoid (CS) coils for full inductive plasma start. High plasma density is demanded from the viewpoints of the power exhaust and reduction in the fuel dilution. For the primary plasma design (JA DEMO 2014) as shown in Table 1, high Greenwald density fraction of $f^{GW} = \bar{n}_e/n^{GW} = 1.2$ ($n^{GW} = I_p/\pi a_p^2$ [10^{20} m^{-3}, MA, m]) was assumed since I_p and line-averaged density ($\bar{n}_e$) were restricted to 12.3 MA and 7.9x10^{19} m^{-3}, respectively. Further increase of c_{Ar}^{main} reduced P_{fusion} lower than 1.5 GW-level due to the fuel dilution, and, at the same time, $HH_{98(y,2)}$ higher than 1.3 was required. Therefore, c_{Ar}^{main}, P_{rad}^{main} and f_{rad}^{main} were restricted up to 0.25%, 82 MW and 0.22, respectively.

JA DEMO higher-κ design increased I_p to 13.5 MA and $\bar{n}_e$ to 8.6x10^{19} m^{-3}, and also improved the plasma performance such as P_{fusion} and τ_E. Thus, the baseline requirements ($HH_{98(y,2)} = 1.3$, $\beta_N = 3.4$) for the steady-state DEMO plasma can be obtained under the higher condition of $c_{Ar}^{main} = 0.6\%$, as shown in Fig. 1(c) and Table 2: P_{heat} becomes comparable to that of EU DEMO1, P_{rad}^{main} is largely increased to 177 MW, and P_{sep} is rather reduced from 294 MW (DEMO 2014) to 258 MW, which has an enough margin above P_{LH} ($f_{LH} = 2.2$). Therefore, the power exhaust concept of f_{rad}^{main} ~0.4 with $HH_{98(y,2)} = 1.3$ (both are slightly higher than ITER-level) and large P_{sep}/R_p (~30MWm^{-1}) is a challenge for both the main plasma and divertor performances. The power exhaust parameters for both JA DEMO designs are shown in Fig. 2, where some representative results of f_{rad}^{main}~0.4 and detached divertor experiments in JT-60U long-pulse Ar seeding were plotted [34]. Here, vertical stability of the high κ_{95} plasma was sustained by passively induced current in the conducting structures without in-vessel control coils. Increasing κ_{95} from 1.65 to 1.75 required improvements of the conducting shell design such as increasing the electrical conductance (shell width) and installing an additional shell behind the inboard BBs [35].

Since n^{GW} for both DEMO designs are lower than that of ITER (1.1x10^{20} m^{-3}), H-mode operation with high $f^{GW} > 1$ is required to satisfy appropriate P_{fusion} and P_{net}. On the other hand, recent experiments (JET-ILW and AUG) reported the restriction at high-f^{GW} (0.9-1) to obtain H-mode plasmas only by external gas fueling [36]. A relatively peaked profile of n_e and a pedestal density of less than n^{GW} will be necessary for the DEMO plasma to obtain the high f^{GW}, and an internal transport barrier (ITB) of the T_e and T_i profiles as well as the n_e profile will

be maintained, in particular, for the JA DEMO plasma to achieve higher $HH_{98(y,2)}$ and β_N.

A plasma performance for the first target of CFETR steady-state scenario was proposed [19], focusing on the tritium breeding; P_{fusion} ~1GW and keeping stable β_N (2.0) and high $HH_{98(y,2)}$ (1.4) at relatively low $\bar{n}_e$ (6.2x10^{19} m^{-3}) and f^{GW} (0.67), which challenges the high-κ plasma design actively controlled by in-vessel coils. Power exhaust result is shown in Table 2. Power handling of large P_{sep} (219 MW) and P_{sep}/R_p (30 MWm^{-1}) is required in the divertor due to low f_{rad}^{main} (0.28), as shown in Fig. 2. Further improvement of β_N (~3.0) will achieve high bootstrap current fraction (f_{BS} ~0.75) as the DEMO level performance of P_{fusion} ~2GW with increasing $\bar{n}_e$ up to n^{GW}. In addition, corresponding hybrid operation scenario with ohmic heating fraction of 0.3, aiming for slightly reducing $HH_{98(y,2)}$ (~1.2) and increasing $\bar{n}_e$ (f^{GW} = 0.85) for the comparable P_{fusion}, reduces P_{sep} (177 MW) and P_{sep}/R_p (25MWm^{-1}) with the same f_{rad}^{main}.

First phase of the K-DEMO (R_p = 6.8m, P_{fusion} = 2.2 GW) steady-state concept proposed to increase f_{rad}^{main} ~0.4 in order to handle the large P_{heat} ~ 600 MW [21] and to achieve the high plasma performance with high f_{BS}, i.e. $HH_{98(y,2)}$ = 1.2, β_N = 2.8, f_{BS} = 0.77 [7]. FNSF long pulse scenario proposed relatively low f_{rad}^{main} = 0.24 for $HH_{98(y,2)}$ ~1, β_N = 2.6, f_{BS} = 0.52 [8]. While P_{sep} (360 and 177 MW) was different, P_{sep}/R_p became large (53 and 37 MWm^{-1}, respectively), which were 2.3-3.3 times larger than that of ITER. Thus, the double null plasma configuration was chosen to distribute the large P_{sep} to the upper and lower divertors.

Consequently, in the recent DEMO-level power exhaust, P_{heat} is 2-4 times larger than that of ITER, exhaust scenario of the large thermal power both in the main plasma and divertor is a common high priority issue. Representative concepts of increasing f_{rad}^{main} with the high plasma performance ($HH_{98(y,2)}$, β_N, f_{BS}) are summarized for the DEMO missions, which determine power handling in the divertor. At the same time, we should design adequate performance of the power handling and particle exhaust in the relatively low density DEMO plasmas. Design improvement to the high plasma density is demanded from the viewpoints of reduction in the fuel dilution, and the power exhaust in the main plasma and divertor.

3. Power exhaust simulation for DEMO divertor design

3.1 Divertor simulation codes and conditions

Conventional designs of DEMO divertor have been developed, based on the ITER divertor. Large power handling of P_{sep}/R_p ~30 MWm^{-1} is an important challenge for JA DEMO and CFETR, and similar size of a long leg divertor (L_{div} = 1.6-1.7 m, i.e. 1.6-1.7 times longer than ITER) is proposed as shown in Fig. 3(a) and (b), respectively. For the JA DEMO divertor, the

poloidal angle between the separatrix and target surface at the strike point (θ^{div}) is designed as 30° and 25° at the inner and outer targets, respectively. The magnetic flux expansion along the target, i.e. $f_{exp}^{div}/sin\theta^{div}$ where $f_{exp}^{div} = (B_p/B_T)^{mid}/(B_p/B_T)^{div}$, is similar (12) at the inner and outer targets. The inner and outer divertors cover all divertor plasma volume, and the SOL field lines within the outer midplane radius (r^{mid}) of 4 cm is contacted to the inner and outer divertors. The outer target angle of CFETR is smaller than those of the JA DEMO and ITER, thus compression of the neutral particles and efficient formation of the plasma detachment will be expected particularly near the strike-point. Design concept of the ITER divertor is simplified for the EU DEMO in order to increase the BB volume, i.e. baffles are removed and targets cover near the strike-points. The long leg divertor with similar θ^{div} at the outer strike point with the open geometry is planned as shown in Fig. 3(c). In addition, instead of the dome structure, a shielding liner is installed in the private region to cover the exhaust opening against neutron flux.

Divertor plasma performance has been simulated with Ne or Ar impurity seeding for DEMO. Figure 3 also shows calculation mesh for the divertor simulations of SONIC on the JA DEMO divertor [13], SOLPS5.0 on the CFETR divertor [19], and SOLPS-ITER on the EU DEMO1 divertor [16]. Studies of longer leg divertor and activating drifts effects on the CFETR divertor were performed by SOLPS-ITER [20], and both the inner and outer leg lengths were recently extended (1.6 m and 2.4 m, respectively). For the EU DEMO simulation, shielding liner is removed in this work. Exhaust power (P_{out}) and particle flux were given at the core-edge boundary; P_{out} = 250, 200, 150 MW for above reference cases, and P_{sep} = 235, 193, 148 MW, respectively, which were slightly smaller than P_{out} since the radiation loss in the plasma edge is less than 7% of P_{out}. Application of the ion and electron diffusion coefficients on the heat flux (χ_i, χ_e) and particle flux (D) for the SOL plasma is a critical issue to simulate the divertor performance. Representative power exhaust parameters and diffusion coefficients are summarized in Table 3. For the JA DEMO, $\chi_i = \chi_e$ = 1 m^2s^{-1} and D = 0.3 m^2s^{-1} were the same as the "standard" values of ITER simulation by SOLPS4.3 [37]. The e-folding length near the outer midplane separatrix ($\lambda_{q//}^{mid}$) of the parallel heat flux ($q_{//}$) profile (including electron and ion components) corresponded to 2.9 mm, which was narrow compared to 3.6 mm in the ITER simulation due to higher T_e^{sep} and T_i^{sep} in the JA DEMO (370 and 830 eV, respectively). While the same χ and smaller χ = 0.18 m^2s^{-1} were given for CFETR and EU DEMO1, respectively, typical $\lambda_{q//}^{near}$ is provided to similar value of ~3mm. For the UEDGE simulation on the FNSF divertor [22], half power of P_{sep} (0.5x176 MW) was assumed to transport to the lower divertor and smaller χ = 0.5 m^2s^{-1} provided smaller $\lambda_{q//}^{mid}$ ~2 mm. On the other hand, $\lambda_{q//}^{mid}$ was scaled

by $\lambda_{q//}^{Eich} = 0.7 \cdot B_t^{-0.77} \cdot q_{95}^{1.05} \cdot P_{sep}^{0.09}$ [mm, T, MW] [38] based on experiment database of the heat load profiles under the attached divertor condition, and the scaling predicted $\lambda_{q//}^{Eich}$ = 0.9 and 1.2 mm for ITER and JA DEMO, respectively. Similar to the ITER case, $\lambda_{q//}^{mid}$ used for DEMO simulations is also wider than the empirical scaling. Reductions of both χ and D to 1/2 and 1/4 produced smaller $\lambda_{q//}^{mid}$ of 1.6 and 1.2 mm, respectively, in ITER simulations [37] and the peak $q_{//}$ became larger. On the other hand, increase of the peak q_{target} remained slightly (20-40%) due to enhancement of the particle recycling near the divertor separatrix. Influence of reducing the diffusion coefficients for the JA DEMO simulation is shown and discussed in Sec. 3.5.

3.2 Plasma detachment and divertor operation at low density

A simple formula of the target heat load by the plasma (q_t^{plasma}) is described by P_{sep}, $f^*_{rad}{}^{div}$, $\lambda_{q//}^{mid}$ and the flux expansion along the target ($sin\theta^{div}/f_{exp}^{div}$), as following, $q_t^{plasma} = (P_{sep}/R_p) \cdot (1-f^*_{rad}{}^{div}) \cdot (sin\theta^{div}/f_{exp}^{div}) \cdot (4\pi\lambda_{q//}^{mid} D^{det})^{-1}$, where power reduction in the detachment is represented by a dissipation factor (D^{det}). Integrated divertor simulation provides two dimensional transport solution of the plasma, neutral and impurity in the divertor. P_{sep}, $f^*_{rad}{}^{div}$ and diffusion coefficients are important key parameters for the divertor performance. In particular, for the large P_{sep}/R_p DEMO design, larger $f^*_{rad}{}^{div}$ is required compared to that of ITER (0.5-0.6). Simulation study will provide appropriate divertor size and geometry to maintain the large radiation peak in the divertor chamber. At the same time, n_e^{sep}/n^{GW} was reported to be ~1/3 in the H-mode plasma experiments [39, 40] and similar fraction in "standard" ITER simulations [37]. A recent experiment result was also lower than critical values of 0.4–0.5 [41], which was consistent with the edge ballooning stability model. As a result, the operation range of n_e^{sep}/n^{GW} is expected to be 0.3–0.5, thus the operation boundary will be investigated in the lower density range of n_e^{sep} = 2 - 3.5x10^{19} m^{-3}, compared to that of ITER. Representative JA and EU DEMO results are mainly shown as different power exhaust concept and divertor geometry.

Divertor operation in the low n_e^{sep} range and influences of the key parameters were recently investigated in JA DEMO [13]. A series of n_e^{mid} scan was performed with changing fuel gas puff and divertor pumping rates (2-10x10^{22} Ds^{-1}), where Ar seeding rate was controlled to keep a given $f^*_{rad}{}^{div}$ value. Two reference series for "JA DEMO higher-κ" (Case-1: P_{sep} ~235MW and $f^*_{rad}{}^{div}$ ~0.8) and "JA DEMO 2014" (Case-2: P_{sep} ~283MW and the same $f^*_{rad}{}^{div}$), and severe condition with reducing $f^*_{rad}{}^{div}$ to ~0.7 for the two references (Case-3 and Case-4) were investigated. Above power exhaust parameter, $P_{sep} \cdot (1-f^*_{rad}{}^{div})$, corresponds to 50, 60, 75 and 90 MW, respectively. Figure 4 (a) (b) show distributions of the radiation power density (W_{rad}) in

the inner and outer divertors at $n_e^{sep} = 2.0 \times 10^{19}$ m^{-3} for Case-1, corresponding to a near lower boundary of the n_e^{sep} range. Total radiation powers in the two divertors are comparable, i.e., 79 and 82 MW, respectively. The large radiation peaks near the separatrix are maintained at the upstream on both divertor legs. In the inner divertor, a large W_{rad} is seen at 40–60 cm upstream of the target near the separatrix, and it is maintained far above the inner target. T_e is decreased to ~1 eV over most of the area of the target, which we describe as "full detachment", as shown in Figure 4 (c). Total heat load (q_{target}) is evaluated by including surface recombination of the ions ($q_t^{rec} = n_i^{div} C_s^{div} E_{ion}$, where n_i^{div}, C_s^{div} and E_{ion} are ion density, sound velocity at the divertor sheath and recombination energy, respectively), radiation power load (q_t^{rad}) and neutral flux load including charge exchange and volume recombination processes (q_t^{n}), in addition to the plasma heat flux (q_t^{plasma}). Multi-peaks appear near the strike-point in the q_{target} profile as shown in Figure 4 (e), which are attributed to peaks of n_e^{div}, n_i^{div}, T_e^{div} and T_i^{div} profiles. The largest peak q_{target} of 4.2 MWm^{-2} is seen in the detached region, mostly attributed to q_t^{rec}. In the outer divertor, a large W_{rad} is also seen at the upstream (40–60 cm) near the separatrix, where local c_{Ar} (= n_{Ar}/n_i) is increased up to 2%. On the other hand, the W_{rad} peak shifts toward the target at the outer flux surfaces as shown in Figure 4 (b), and it becomes smaller than 10 MWm^{-3} (lowest color bar) and located just above the target (a few cm). The plasma detachment is produced within ~12 cm near the strike-point as shown in Figure 4 (d), which we describe as "partial detachment". The peak q_{target} of 5.5 MWm^{-2} is seen at the boundary of the attached region, where both T_e^{div} and T_i^{div} are increased from 1–2 to ~15 eV, and n_e^{div} is decreased from ~1.5× 10^{22} m^{-3} to ~1.5 x10^{21} m^{-3}. Thus, the peak q_{target} is sensitive to their profiles. At the same time, since the W_{rad} peak shifts toward the target, q_t^{plasma} and q_t^{rad} become dominant. In the partial detachment, the peak q_{target} is sensitive to the plasma temperature and density profiles and location of the W_{rad} peak.

The peak q_{target} is generally larger than that of the inner q_{target}. Divertor operation for the outer peak q_{target} in the low n_e^{mid} range and influences of the key parameters were summarized in Fig. 5. Closed circles show a series of Case-1, where the reference shown in Fig. 4 is marked by open circle. Squares, triangles and diamonds show other three series of Case-2, Case-3 and Case-4, respectively. The peak q_{target} is reduced with increasing n_e^{sep}, and increased with increasing $P_{sep}\cdot(1\text{-}f^{*}_{rad}{}^{div})$. As a result, two references of Case-1 and Case-2 are acceptable in the low $n_e^{sep} \geq 2$x10^{19} m^{-3} to reduce $q_{target} \leq$10MWm^{-2}. On the other hand, for the Case-2, the peak q_{target} is increased from 5.6 (Case-1) to 9.5 MWm^{-2} at $n_e^{sep} = 2$x10^{19} m^{-3} with reducing width of the plasma detachment to 10 cm. Since the surface temperature of the tungsten target is reduced in Case-1 (JA-DEMO higher-κ), compared to Case-2 (JA DEMO 2014), it has

advantages to provide enough operation margin to the recrystallization temperature (~1200°C). For the lower $f^{*}_{rad}{}^{div}$~0.7 cases (Case-3 and Case-4), the detachment width is further decreased, and the peak q_{target} is seen also at the attached region. The peak q_{target} is further increased to 12.2 and 14.5 MWm^{-2}due to the increase in $q_t{}^{plasma}$, where both the local $T_e{}^{div}$ and $T_i{}^{div}$ are increased. Higher $n_e{}^{sep}$ operation (larger than $2.3x10^{19}$ and $2.6x10^{19}$ m^{-3}) is acceptable for Case-3 and Case-4, respectively. For all cases, Ar concentrations in the midplane SOL ($c_{Ar}{}^{mid} = n_{Ar}{}^{mid}/n_e{}^{mid}$) are reduced to 0.4-1% in $n_e{}^{sep}$ = 2.0-2.5x10^{19} m^{-3}.

Divertor plasma performance for EU DEMO divertor has been investigated, using SOLPS-ITER. Reductions in $T_e{}^{div}$ and q_{target} were investigated with increasing the Ar seeding rate (0.2-2x10^{21} Ar・s^{-1}) at relatively large gaff puff rates such as an order of 10^{23} D・s^{-1}. Radiation loss distribution in the divertor, plasma profiles and accumulated heat load profiles in the inner and outer targets for the representative result are shown in Fig. 6, where $n_e{}^{sep}$ ~2.8x10^{19} m^{-3} is higher than that of the JA DEMO and Ar seeding rate of 1.5x10^{21} Ar・s^{-1}. P_{sep} is 146 MW, which is slightly less than P_{out} of 150MW. Total line radiation is 75 MW, and distribution in the divertor is shown in Fig. 6 (a). While $f^{*}_{rad}{}^{div}$ = 0.51, it is noted that neutron dissipation processes by charge exchange and recombination processes become 49 MW maybe by large fuel gas puff. Thus, total volumetric energy losses from the plasma becomes 0.85. Large W_{rad} is seen along both inner and outer divertor legs near the separatrix. In the inner divertor, $T_e{}^{div}$ is 0.4 – 3.5 eV as shown in Fig. 6 (b): full detachment is produced over wide region. The peak q_{target} (2.0 MWm^{-2}) appears at r^{div} =10 cm, where not only $q_t{}^{rec}$ but also $q_t{}^{rad}$ are dominant (0.9-1 MWm^{-2}) due to large W_{rad} extended above the inner target in this case. Here, $q_t{}^{n}$ is not presented, which will be larger contribution (1-2 MWm^{-2}). On the other hand, in the outer divertor, partial detachment is produced in $r^{div} \leq 8$ cm, and $T_e{}^{div}$ is increased up to 24eV in the attached region as shown in Fig. 6 (d). For the EU DEMO simulation, peak q_{target} (2.3 MWm^{-2}) appears in the detached region near the detach-attach boundary, and the local $T_e{}^{div}$ is 1-2 eV. Thus, $q_t{}^{rec}$ is dominant (1.3 MWm^{-2}) and both $q_t{}^{plasma}$ and $q_t{}^{rad}$ are relatively small (0.4-0.5 MWm^{-2}). Provided that further contribution of $q_t{}^{n}$ is added, total peak q_{target} is increased by 1-2 MWm^{-2} (~4 MWm^{-2}). While the peak q_{target} is produced in the detached region, the value is sensitive to the $T_e{}^{div}$, $T_i{}^{div}$ and $n_e{}^{div}$ profiles near the detach-attach boundary.

Systematic study of the plasma detachment was recently performed with higher $n_e{}^{sep}$ ~4x10^{19} m^{-3} assuming larger ion flux by pellet fueling at core-edge boundary [18]. Peak $T_e{}^{div}$ at the outer target is reduced with increasing Ar seeding rate as shown in Fig. 7(b), and full detachment is produced even in the outer divertor at Ar seeding rate of 6x10^{20} Ar・s^{-1}. At the same time, the

total radiation loss also becomes the maximum, and $f^*_{rad}{}^{div}$ and ion flux to the target were rather decreased with further increasing Ar seeding due to increasing P_{rad} in the edge plasma (as described in "core" in Fig. 7(a)). Since large radiation loss is not maintained in the divertor region, Ar seeding rate and $f^*_{rad}{}^{div}$ are restricted below $6\text{x}10^{20}$ Ar·s^{-1} and ~0.7. On the other hand, the total energy loss would be enhanced by neutral dissipation.

3.3 Effects of divertor geometry and drifts

Vertical target design was applied for the ITER divertor from the viewpoints of producing the plasma detachment near the separatrix at lower $n_e{}^{sep}$ and the wider operation range without building up the X-point MARFE [42]. Since year-long level steady-state operation is expected for the DEMO divertor, reductions of peak $T_e{}^{div}$ (and $T_i{}^{div}$) as well as the peak q_{target} are required to minimize erosion of the W-target under the partial detached divertor.

Effects of the target angle (θ^{div}) on the detachment plasma and peak q_{target} were investigated in FNSF divertor by UEDGE code with neutral/gas fluid modelling [22]. The vertical target geometry ($\theta^{div} = 25°$) was a baseline design similar to ITER, and the inner and outer L_{div} were 0.37 m and 0.60 m, respectively. Further open geometries ($\theta^{div} = 40°$ and 70°) were compared as shown in Fig.8 (a), where the flux expansion at the target was decreased. Lower divertor performance was simulated with a half power of P_{sep}, i.e. 88 MW. Thus, ITER-level power exhaust ($0.5P_{sep}/R_p = 18$ MWm^{-1}) was required in the shorter leg divertor. Ne seeding was used, and relatively high n_e ($1\text{x}10^{20}$ m^{-3}) was given at the core-edge boundary ($r^{mid}/a_p = 0.97$). Total radiation fraction by Ne and hydrogen isotopes (D/T) correspond to $f^*_{rad}{}^{div} = P_{rad}{}^{div\text{-}low}/(0.5P_{sep})$ = 0.83. For the baseline case, as shown in Fig. 8 (b-d), the partial detachment is produced at the outer target, and the peak q_{target} (~5 MWm^{-2}) can be reduced in the attached region (r^{div} ~0.3 m), which is attributed mainly to $q_t{}^{plasma}$ (~4 MWm^{-2}), while relatively high $T_e{}^{div}$ of ~60 eV is seen at the outer location (r^{div} = 0.5-0.7 m). Here, heat load components by electron and ion/atom transports are separately shown, and the latter includes charge exchange and volume recombination processes ($q_t{}^n$). In addition, q_{target} is increased to ~3 MWm^{-2} and $T_e{}^{div}$ = 2-3 eV between the detach-attach boundary and the peak q_{target} (r^{div} = 0.15-0.25 m) as shown in Fig. 8 (d), where $q_t{}^{rad}$ (~1.5 MWm^{-2}) is the major heat load compared to the other components ($q_t{}^{plasma} + q_t{}^n + q_t{}^{rec}$) due to significant radiation peak neat the target. It was also noted [22] that kinetic transport modelling of neutral and molecule (self-consistent coupling of UEDGE and DEGAS result) is required for accurate evaluation, which extends the low $T_e{}^{div}$ region and further reduces the q_{target} peak.

For the open geometry case (θ^{div} = 70°), detached region becomes wider, and peak q_{target} appears at the detached region similar to the inner divertor (nearly full detachment). Thus, the peak q_{target} is decreased to 3.5 MWm^{-2}, where q_t^{rad} (~2 MWm^{-2}) is the major heat load due to reduction of the plasma transport component. Operation window of the wide detachment and low peak q_{target} is important to choose the divertor geometry. At the same time, transport modellings of desorption process, elastic collisions and kinetic effects become important to evaluate the peak q_{target} and impurity distribution in the nearly full detached divertor. Further studies will continue by self-consistent simulation of UEDGE and DEGAS2.

Appropriate divertor L_{div} for the vertical target design is primarily determined to maintain the seeding impurity and large radiation peak in the divertor. Divertor performance with L_{div} = 1.6-1.7 m has been investigated for the high P_{sep}/R_p handling such as JA DEMO (30-35 MWm^{-1} by Ar seeding) [13, 14] and CFETR (28 MWm^{-1} by Ne seeding) [19], and these results demonstrated to be appropriate for their reference design. Further study was recently performed for CFETR by SOLPS-ITER with various drifts activated such as $\nabla B \times \boldsymbol{B}$ and $\boldsymbol{E} \times \boldsymbol{B}$, which produced inboard-enhanced asymmetry of the particle flux profile and outboard-enhanced heat load profile [20]. Extension of L_{div} was proposed, and effects on the plasma detachment and impurity retention in the divertor were investigated. Geometries of the refence and longer leg divertors are shown in Fig. 3 (b) and 9 (a): both inner and outer L_{div} were extended from 1.3 m and 1.7 m to 1.6 m and 2.4 m, respectively, inner θ^{div} was increased from 34° to 46°, and outer θ^{div} was the same (20°) [43]. P_{out} from the core-edge boundary was the same (200 MW) as the previous study, but radial distributions of χ and D were introduced, where χ was reduced to 0.5 m^{2}s^{-1} inside the separatrix (r^{mid} = -5 - 0 cm) and increased to 2.0 m^{2}s^{-1} in far SOL region (r^{mid} = 3 - 6 cm): D was similarly varied. Typical $\lambda_{q//}^{mid}$ was ~4 mm and n_e^{sep} = 3.7x10^{19} m^{-3} in the series of calculations. Comparison between Ne and Ar seedings showed that divertor cooling by the Ar seeding was efficient, thus the Ar seeding was chosen for the baseline scenario.

Under a comparable condition of the gas puff (4x10^{22} D·s^{-1}) and Ar seeding (4x10^{19} Ar·s^{-1}) with drifts activated, poloidal distributions of T_e and c_{Ar} near the separatrix from the outer midplane SOL to the target are compared in Fig. 9 (b) (c), respectively. For the reference case, the target plasma becomes attached (T_e^{div} = 230 eV) due to lower radiation loss in the outer divertor, while the detachment is produced for the longer leg case (T_e^{div} = 3 eV). Next, similar poloidal distributions of T_e are achieved with increasing Ar seeding (1x10^{20} Ar·s^{-1}) only for the reference case as shown in Fig. 9 (d)(e), where $f^*_{rad}{}^{div}$ ~0.7 is comparable and similar partial detachment is produced near the separatrix (Fig. 9 (f)(g)). For the longer leg case, peak T_e^{div} at

r^{div} ~ 0.35 m in the attached region is reduced from 47 eV (reference case) to 34 eV while reduction in the peak q_{target} is small. As a result, the longer leg is new baseline design in order to reduce both the peak q_{target} and T_e^{div}, c_{Ar} in SOL and edge regions and to extend the divertor operation window at lower n_e^{sep}, provided that drifts affect the divertor performance.

Reduction in the peak q_{target} by N_2, Ne or Ar seeding was investigated in the double-null divertor for K-DEMO (by UEDGE) [21] with ITER-level leg length and larger power to either divertor, i.e. $0.5P_{out}$ = 300 MW. Results showed that Ar seeding enhanced partial detachment more than those of Ne and N_2 seeding cases, and the peak q_{target} was efficiently reduced. It is noted that appropriate power handling (q_{target} ≤10 MWm^{-2}) was restricted only by reducing the pumping speed, i.e. increasing the albedo of the divertor pumping to 0.99945. Since the operation window of the detachment is restricted, further improvements of the geometry and the power exhaust scenario both in the main plasma and divertor will be required.

3.4 Estimation of W-erosion in the partial detachment

Net erosion of the W target becomes life-time issue for the DEMO divertor since the ion fluence is expected to be one order of magnitude larger than ITER. Low T_e^{div} and T_i^{div} plasma is preferable in the partial detached divertor, in particular, for the vertical target geometry. Estimations of W-flux and W-erosion rate are summarized in Table 4. W-erosion is enhanced mainly by seeding impurity at the attached region, where the local T_e^{div} is increased to 20 - 40 eV while incident ion flux (Γ_i^{div}) is reduced at the outer r^{div}. Gross W-sputter flux in the DEMO divertor simulation is sensitive to local plasma condition of Γ_i^{div} and impurity concentration (c_z) as well as T_e^{div}. Typical values of gross W-sputter flux ($Y_Z \cdot c_z \cdot \Gamma_i^{div}$, Y_Z is sputter yield) are reported between $6.3\text{x}10^{17}$ and $8\text{x}10^{19}$ $W \cdot m^{-2}s^{-1}$, where TRIM code surface database was used for the EU DEMO result (the small one) [44]. Net erosion rate is estimated by a simple formula of Δd_{sec} (nm/s) = $10^3 \cdot R_{net} \cdot (Y_Z \cdot c_z \cdot \Gamma_i^{div})/[6.02\text{x}10^{26}/183.8 \cdot \rho] = 1.57\text{x}10^{-20} R_{net} \cdot Y_Z \cdot c_z \cdot \Gamma_i^{div}$, where R_{net} is the ratio of net to gross erosion rate and ρ is W mass density ($19.3\text{x}10^3$ kgm^{-3}). R_{net} is also a critical factor, and 0.1 is given for the FNSF estimation, which considers prompt redeposition (finite-Larmor) effect [45]. The same R_{net} is assumed for other cases. Prompt and local deposition modelling such as the finite-Larmor effect and friction force by the plasma flow, and experiment database for gross to net erosion ratio are demanded. Net erosion depth for year-long operation is also estimated as Δd_{year} (mm/year) = $4.95\text{x}10^{-19} R_{net} \cdot Y_Z \cdot c_z \cdot \Gamma_i^{div}$, which is a few 10 times larger than that of ITER (e.g. 2500 pulses of 400 s discharges per year). Some results suggest that Δd_{year} reaches 1mm-level, which corresponds to 10-20% of the monoblock

thickness. As a result, simulation results in the vertical target geometry suggested further reduction of both peak T_e^{div} and T_i^{div}, and "pronounced detachment" (~5eV) as shown in ASDEX-upgrade [46] is preferable. Operation at higher n_e^{sep} or/and sweep of the strike-point location [26, 47] will be considered.

3.5 Effects of diffusion coefficients on power exhaust

In the divertor simulation, radial diffusion coefficient of the SOL plasma is a primary key parameter to determine profiles of the heat and particle fluxes. For the recent DEMO simulations, $\lambda_{q//}^{mid}$ of the total (electron and ion) $q_{//}$ profile was similar value of ~3 mm, except that $\lambda_{q//}^{mid}$ ~2 mm for the FNSF divertor, while different diffusion coefficients were used as shown in Sec. 3.1 and Table 3. Effects of smaller $\lambda_{q//}^{mid}$, which was produced by reducing diffusion coefficients, on the partial detachment and divertor operation were investigated in JA DEMO [13, 14]. Some representative simulations with reducing both χ and D to half values, i.e. $\chi_e = \chi_i = 0.5$ m^{2}s^{-1} and $D = 0.15$ m^{2}s^{-1}, were performed for the four series as shown in Sec. 3.2. Profiles of electron, ion and total parallel heat fluxes near the X-point ($q_{//e}^{Xp}$, $q_{//i}^{Xp}$ and $q_{//e}^{Xp}+q_{//i}^{Xp}$) for Case-1 ($P_{sep}$ ~235MW, $f^*_{rad}{}^{div}$ ~0.8 and the same n_e^{sep} of 2.0x10^{19} m^{-3}) are compared in Fig. 10 (a)(c), mapping to the outer midplane radius (r^{mid}). Here, radial gradients of T_e^{Xp}, T_i^{Xp} and n_e profiles were generally increased with reducing χ and D, and increase in T_i^{Xp} (from 820 to 1190 eV for the same n_e^{sep} cases) was significant due to reduction in n_e^{Xp} in the SOL region. Both $q_{//e}^{Xp}$ and $q_{//e}^{Xp}+q_{//i}^{Xp}$ profiles are described approximately by a two-exponential function such as $q_{//}(r^{mid}) = q_{//}^{near} exp(-r^{mid}/\lambda_{q//}^{near}) + q_{//}^{far} exp(-r^{mid}/\lambda_{q//}^{far})$, where $\lambda_{q//}^{near}$ and $\lambda_{q//}^{far}$ are e-folding lengths of "near-SOL" and "far-SOL", and the former is mostly attributed by the electron conductive transport. $\lambda_{q//}^{near}$ values of $q_{//e}^{Xp}$ and $q_{//e}^{Xp}+q_{//i}^{Xp}$ profiles become smaller (from 2.3 to 1.6 mm and from 2.9 to 2.2 mm, respectively) mainly due to reduction of the radial diffusion and enhancement of the parallel conductive transport. Reference [14] (Fig. 6 (e)) showed that $\lambda_{q//}^{near}$ values of four representative $q_{//e}^{Xp}+q_{//i}^{Xp}$ profiles for the different P_{sep} and $f^*_{rad}{}^{div}$ cases were 1.2–1.6 times larger than those for the $q_{//e}^{Xp}$ profiles, and they were decreased from 2.5–3.3 mm (for the reference χ and D) to 1.7–2.2 mm.

On the other hand, transition from the "near-SOL" to the "far-SOL" in the $q_{//e}^{Xp} + q_{//i}^{Xp}$ profile is attributed to $q_{//i}^{Xp}$ profile, i.e. ion transport. Simulation results suggested that "flow reversal" [48] is produced above the outer divertor target by locally increasing neutral ionization and plasma pressure, and that it is extended to the low-field-side SOL as shown in Fig. 10 (b)(d). Thus, the convective transport is also driven from the outer divertor to the

upstream in the wide SOL region, which is not included in *the* $q_{//i}^{Xp}$ *towards the outer divertor*. Flat "shoulder" appears in the $q_{//i}^{Xp}$ profile with increasing *the convective heat flux towards the outer divertor*, and the transition from the "near-SOL" to the "far-SOL" is emphasized in the $q_{//e}^{Xp} + q_{//i}^{Xp}$ profile. It is noted that the transition location in the $q_{//e}^{Xp} + q_{//i}^{Xp}$ profile moves from r^{mid} ~1.1 to 0.7 cm, which corresponds to the flux surface of the detach-attach boundary (shifted from r^{div} = 12 to 7 cm, respectively). At the same time, the peak q_{target} was produced in the attached region, and the peak is increased from 5.8 to 9.5 MWm^{-2} mostly due to large increases in the local T_e^{div} and T_i^{div}. These simulation results suggested that the $q_{//i}^{Xp}$ profile modified by the "flow reversal" formation significantly affects the partial detachment profile and the peak q_{target}.

Results of the peak q_{target} at the outer target for the smaller χ and D cases are added by open symbols in Fig. 11. Similar to those in Sec. 3.2, the peak q_{target} is increased with increasing $P_{sep}\cdot(1\text{-}f^*_{rad}{}^{div})$ and they are reduced with increasing n_e^{sep} for each case. Lower boundary of n_e^{sep} for q_{target} ≤10MWm^{-2} is determined to be 2.0x10^{19} and 2.3x10^{19} m^{-3} for the reference $f^*_{rad}{}^{div}$ (~0.78) cases: P_{sep}=235 and 283 MW, respectively. Therefore, the reference $f^*_{rad}{}^{div}$ cases are acceptable in the low n_e^{sep} operation, where higher n_e^{sep} (≥ 2.3x10^{19} m^{-3}) is required for the latter case. On the other hand, for the lower $f^*_{rad}{}^{div}$ (~0.67) cases, the peak q_{target} and n_e^{sep} are significantly increased with decreasing the partial detachment width and increasing the local T_e^{div} and T_i^{div}. Thus the divertor operation is difficult in the low n_e^{sep} range. As a result, the reduction in χ and D significantly affected the divertor power exhaust due to increase of the $q_{//i}$ profile as well as the dominant $q_{//e}$ near the separatrix. In order to produce the detachment plasma at the significantly large $q_{//}$ region and to reduce the peak q_{target} ≤10MWm^{-2}, high $f^*_{rad}{}^{div}$ of 0.8 level was necessary for the JA-DEMO designs.

4. Divertor target and heat removal design

4.1 Design concepts and key design parameters

Conceptual designs of the plasma facing components (PFCs) and coolant routing in the divertor cassette have been developed based on the divertor simulation results. Since steady-state power handling of 10 MWm^{-2}-level peak heat load is a common requirement for the conventional divertor design, the water-cooled target of the ITER technology, i.e. W-monoblock (W-MB) and Cu-alloy (CuCrZr) cooling pipe [24], is a primary baseline concept. On the other hand, engineering design adequate for higher neutron irradiation condition is required for the DEMO design. Recent design concepts are summarized in Table 5, and designs

of the divertor PFC units and cassette body (CB) for EU DEMO, JA DEMO, CFETR and K-DEMO are shown in Fig. 12. All DEMO concepts have the same number (16) of the toroidal field coils (TFCs), which is less than ITER (18), and the maintenance port is located between TFCs. Three adjacent divertor cassettes are replaced through one maintenance port in EU and JA DEMOs. The divertor geometry for EU DEMO is simplified compared to that of ITER, i.e. baffles are removed, inner and outer target plates cover ~0.7 m near the strike-points and a flat shielding liner is installed to protect the vaccume vessel against high neutron irradiation. Weight of one EU divertor cassette is 8.3 ton, which is comparable to that of ITER divertor. JA divertor covers most of the divertor plasma below the X-point similar to ITER, thus the total weight of one cassette (~22 ton) is 2.7 times heavier. In order to reduce each cassette weight for CFETR, number of the cassette is increased to 80.

Neutron irradiation doses on W-MB and CuCrZr heat sink are significantly increased in DEMO due to increasing operation time as well as the neutron flux. The maximum doses for a full-power-year (FPY) operation become larger than those for the full operation period of the ITER divertor, which are expected to 0.54 and 2.5 displacements per atom rate (dpa), respectively [53]. Therefore, the engineering design and technology of the divertor component should consider degradation of material properties and reductions of irradiation damage until the scheduled replacement. Since the divertor geometry for EU DEMO is shallow and open, the maximum doses on the W-MB and CuCrZr pipe at the target are 1.9 and 7.2 dpa·FPY^{-1}, respectively, and the former is comparable to those at the baffle for other DEMO divertors. It is noted that doses on the W-MB and CuCrZr pipe near the outer strike point for EU DEMO are expected to ~1 and 2–3 dpa·FPY^{-1}, respectively [50], both of which are larger than ~0.4 and ~1.2 dpa·FPY^{-1} for JA DEMO [27], due to influence of the divertor geometry and larger P_{fusion}. Replacement of the W-MB and heat sink is prefered at the same time as the BB replacement (~3 years). Reduction in the thermal conductivity of the W-MB due to the nuclear transmutation to Re and Os reaching 1-2 wt% at several dpa [53] will be acceptable at the high surface temperature of 500-1200 °C. Further factors to reduce the conductivity and mechanical properties of the armor material, i.e. bulk-W and W-alloy, by neutron irradiation and plasma surface interaction were reviewed [54, 55]. In addition, recrystallization will progress even at lower temperature (~900 °C) for a year-long operation [56, 57], where the peak q_{target} is required to be maintained less than 10 MWm^{-2} in the later period.

Selection of Cu-alloy (CuCrZr and Cu-base composites) as the heat sink for the high heat load target is owing to the excellent thermal conductivity. Design constrains of the power

handling under the neutron irradiation condition are summarized in Table 6. It is firstly determined by the mechanical property at high temperarture (> 280°C) due to radiation induced softening and creep [52, 59]. Corrosion on the inner wall of the pipe above 200°C is another common design issue. At the same time, radiation induced hardening at the lower temparature also starts from the low irradiation dose (~0.2 dpa). Therefore, the coolant temperature (T_{cool}) for the high heat flux component is increased to higher than that of ITER (~70°C). The selection of T_{cool} has large variation between 70 °C and 200 °C (EU DEMO: 130 °C, JA DEMO: 200 °C, CFETR: 140-180 °C, K-DEMO: 70 °C), which will be a critical lifetime issue. For JA DEMO, K-DEMO and recent CFETR divertors, the CuCrZr pipe is used only for the target, and reduced activation ferritic martensitic (RAFM) steel pipe is applied to the heat sink for the higher dose (up to 5–6 dpa·FPY^{-1}) but lower heat load (lower than a few MWm^{-2}) region. JA DEMO anticipates degradation of the mechanical property at the high temperarture, and replacement of the inner and outer targets is expected after 1-2 year long operations, i.e. more frequently compared to the BB replacement.

For EU DEMO (repeating two hour pulse operation), lower T_{cool} (130 °C) is determined mainly by requirement to ensure a safety factor of 1.4 (i.e. 40% margin) to the large critical heat flux (CHF: 45 MWm^{-2}) of the coolant under high heat load of 20 MWm^{-2}, which is also defined as a standard technology target for the high heat load of 10 s pulse. It is tentatively assumed that the key mechanical behavior of the CuCrZr heat sink irradiated for two FPYs would not significantly change at least up to 10 dpa, considering the pronounced mechanical saturation behavior of CuCrZr specimens irradiated and tested at low temperature (150 °C) after a low irradiation dose (≤ 0.6 dpa) [60]. In addition, T_{cool} (130 °C) is lower from the viepoint from the thermal recovery temperature (150–200 °C) of irradiated CuCrZr. Comprehensive database of these properties, design criteria and their improvement are required to determine the life time of the power handling unit.

4.2. Design issues of high heat removal components and coolant condition

Arrangements of plasma facing components and coolant routing for the different DEMO divertor concepts are shortly reviewed, and common design issues are clarified. Arrangement for the JA DEMO divertor and the coolant routes are shown in Fig. 13 (a) and (b), respectively. The total thermal power to the divertor was assumed to be 325 MW, which included about 40% margin above the simulation result (P_{sep}~235MW). In addition, the total volumetric nuclear heating by neutron and γ-ray fluxes (114MW) was considered. Total thermal power to the inner

and outer target components was dominant compared to the nuclear heat, and those to the dome, baffles and reflectors were still larger by the factor of 1.5-3. Heat sink, i.e. CuCrZr or RAFM steel (F82H) pipes, was determined based on neutronics calculation [27]. The W-MB and CuCrZr pipe units were incorporated in the inner and outer targets, which broadly covered the high heat load region of 0.8 m near the both strike-points, and the maximum doses were ~1 and ~1.5 dpa·FPY^{-1}, respectively. Arrangement of the coolant route for the two targets was revised from series to parallel [17] in order to supply the coolant with comparable velocity of 11-12 ms^{-1} (at the inlet of swirled pipe), which reduced the pressure drop (< 1 MPa) at the inner target incorporating smaller number of the W-MB units, i.e. 32 and 43 for the inner and outer units. The parallel distribution concept is also a baseline of the EU DEMO divertor.

For the JA DEMO, relatively high T_{cool} (200 °C) coolant is provided in order to minimize the irradiation embrittlement. Maximum temperatures of W-MB and CuCrZr pipe on the *fish-scale* surface target were evaluated for the steady-state peak q_{target} of ~10 MWm^{-2} and the nuclear heating. The former and latter corresponded to, respectively, ~1190 °C, which was just below the critical temperature of W-recrystallization (~1200 °C), and ~350 °C, where influence of thermal softening on the CuCrZr pipe was somehow fostered above 280-300 °C [62]. Elasto-plastic analysis of the coolant pipe was performed under the higher peak q_{target} of 10 and 15 MWm^{-2}-level, where the latter maximum temperature was increased to ~380 °C. The maximum heat fluxes of 18 and 22 MWm^{-2} were widely distributed on the water side of the pipe, respectively. Since they were 64% and 79% of CHF (28 MW m^{-2}), the high T_{cool} (200 °C) coolant was acceptable for the heat removal. Expansions in the pipe axis (z) and circumferential (θ) directions were seen in the coolant pipe under the MB tile, and compression was caused between MB tiles. While stress (σ_Z)–strain (ε_Z) trace at the maximum stress location showed similar trajectory ($\Delta\sigma_Z$ ~300MPa and $\Delta\varepsilon_Z$ ~0.25%) with repeating the higher heat load cycles. Mechanical toughness of the pipe against thermal softening may not be critical for life time issue at least for unirradiated condition, but it is anticipated with increasing the irradiation dose. The W-MB and F82H pipe unit is arranged at higher neutron irradiation region such as dome, and baffles. Higher T_{cool} and pressurized water (290°C, 15 MPa) similar to the BB design [63] is used for the electricity generation by turbine system similar to a pressurized water fission reactor (PWR). Since maximum heat load to the surface was 1-1.5 MWm^{-2} in the steady-state operation, the coolant route to the dome and reflectors was arranged by a series connection due to reducing the route branches and joints. On the other hand, it is revised to the parallel one in order to exhaust the nuclear heat on the support structures as well as the plasma facing units.

The water-cooled target concept is selected for the EU DEMO as a baseline concept [49, 50, 61], which can take advantages of the thermal conductivity and the thermohydraulic properties compared to helium gas. The divertor configuration and coolant routing have been revised to the one shown in Fig.14 (a) (b) [50]. Total heat load to the plasma facing units (targets, shielding liner and reflection plates) was given to be 200 MW, which is 33% above the simulation value of P_{sep} ~150MW, and volumetric nuclear heating in the plasma facing units and CB was 139 MW. Length of the vertical target (VT) of ~0.7 m was comparable to the JA divertor target (~0.8 m). The coolant route was divided to the inner and outer targets (incorporating 32 and 44 W-MB units, respectively), and the flow velocity was comparable for the both targets (14-16 ms^{-1} in swirled cooling pipe). Inlet T_{cool} was recently reduced from 150 to 130 °C in order to increase CHF to larger than 45 MWm^{-2}. Maximum temperatures of the CuCrZr pipe were evaluated to be ~310 and ~440 °C at the upper location near the strike point for the peak q_{target} of 10 and 20 MWm^{-2}-level, respectively, corresponding to the steady-state and slow transient cases. The former is mostly in the optimal temperature range of 250-300 °C, and the latter is expected to reduction in the yield strength, in particular, under neutron irradiation. Uncertainty and limitations implicit in lifetime projection for the CuCrZr pipe and Cu interlayer have been recently examined by means of finite element method (FEM) simulation, and elasto-plastic analysis for some foreseen problems under repeating the high heat load [64] such as (i) influences of initial residual stress on the cooling pipe and interlayer, (ii) shakedown response of the elasto-plastic structure in the early cycles, (iii) loss of its initial yield strength by ageing (softening by thermal ageing) under the long-term cycles (in particular, exceeding the allowable service temperature limit of ~350 °C). Reduction in the coolant T_{cool} is a trade-off issue under the neutron irradiation condition, but it would be still acceptable (suggested from ITER SDC-IC data) that the total elongation remains larger than 5% in embrittled CuCrZr pipe (for 0.3-5 dpa) at the low temperature, and it could be rather beneficial since the fracture toughness of the pipe (for 0.3-1 dpa) with a sub-mm level crack located at the inner wall is decreased with increasing the temperature (finally no margin at ~350 °C for a large crack case). Furthermore, elasto-plastic analysis was applied to the W-MB unit by using available neutron irradiated material data [63, 64]. Results suggested most likely failure behavior that cyclic strain on the CuCrZr pipe surface was accumulated, in particular, in the gap between W-MBs, leading to early fatigue cracks and potential coolant leaks.

Copper could be hardened and embrittled when transmutation gas bubbles (e.g. helium) are segregated at grain boundaries at higher dose (~6 dpa). Embrittlement of the Cu interlayer leads to substantially higher stresses (tensile stress on the armor), which may cause a crack formation

of the W-MB at or near the bond interface, leading to a local reduction of heat conduction. Distinct consequences of limited knowledge on the actual state of materials and effective loading history were discussed in the light of expected failure modes. Degradation of the mechanical property of heat sink and joint/interlayer caused by radiation induced softening and/or hardening at the lower dpa can be minimized by application of new W and Cu/Cu-alloy target concepts as shown in Sec. 4.3.

CB designs have been developed for EU and JA DEMO divertors to incorporate their power exhaust units and coolant pipes, which will be consistent with reducing the fast neutron flux to protect the vacuum vessel (< 2.75 dpa) and replacement of the power exhaust units [17]. Number of the main coolant pipes is minimized to 4, and inlet and outlet are located at the outboard cassette. The cassette structures and coolant conditions are different, while CB can be made by welding similar RAFM steel (Eurofer97 and F82H). EU CB is composed of a box structure with internal ribs, and it is cooled by higher inlet T_{cool} (180 °C) coolant as shown in Fig. 14 (b)(c), which ensures the entire structure sufficient fracture toughness at the neutron damage (< 6 dpa) [50]. The coolant is also used for the liner and reflectors by a series connection. Although the inlet T_{cool} is low from viewpoint of irradiation embrittlement of the RAFM steel, it was mainly determined by temperature margin (up to 550 °C) of key components such as supports of the reflector plates due to inefficient exhausting local nuclear heat. The issue of tight coolant margin in the liner plate and CB also needs caution. Since the exhaust slot is designed to be at the bottom of the cassette, the liner mainly has a role in reducing the neutron flux to the cassette and the bottom area of the vacuum vessel.

JA CB consists of thick (25 cm) plate structures with two lines of cylindrical coolant puddles in order to reduce the fast neutron and γ-ray flux as shown in Fig. 13 (a). The exhaust slot is located at the outboard bottom in order to reduce the neutron flux to the vacuum vessel. The PWR condition coolant (290 °C, 15 MPa) is provided from the inboard and outboard manifolds through the side routes of the CB to the puddles as shown in Fig. 13 (b), and it finally exits to a manifold near the exhaust slot. The coolant velocity of 1.5 ms^{-1} is enough to remove the total nuclear heat of 0.7 MW in one cassette body, corresponding to totally 32 MW for 48 cassettes.

Divertor configuration and water routing for CFETR have been recently developed [43, 51]. The divertor consists of three plasma facing modules (inner target, dome and outer target) and CB. The coolant routing has been developed from a simple parallel one [43] to a hybrid one [51] as shown in Fig. 15 (a) and (b), respectively. The former design proposed that reflector plate and baffle were connected to the target module. Low T_{cool} (140 °C, 5 MPa) coolant is

provided firstly to the left-half container structure in CB, which is made of SS316L at the first operation stage. Then, it is supplied parallel to inlets of the three modules in order to provide similar flow velocity of 10 ms^{-1} to the inner and outer targets since in-out asymmetry of the W-MB unit numbers (18 and 28, respectively) is larger than those for EU and JA DEMO divertors. The coolant for each module circulates poloidally from the W-MB unit to the module transition support, then returns to the right-half container structure in the CB. Here, the CuCrZr pipe is used for all target and dome modules. A hybrid routing is proposed to improve the heat removal of the outer target more efficient and to apply the W-MB units with RAFM-steel pipes at baffles and dome as explained in the JA DEMO design. The flow scheme is shown in Fig. 15 (c). In the hybrid circuit, inner divertor (IVT) and dome connect in parallel, and outer divertor (OVT) connect them in series. Here, the dome circuit is separated toroidally to two half structures (Dome part I and II), and the coolant circulates through inner reflector, dome and outer reflector of the Dome part I, then it is returned in the Dome part II. Mass flow rates for IVT and Dome are 12.2 and 7.1 kgs^{-1}, respectively. Pressure drop for the two routes is similar (0.79 MPa), and the total drop is 1.95 MPa. The inlet T_{cool} is increased to 180 °C for the RAFM-steel pipe application. Evaluation of the total heat exhaust is in progress, while thermal stress analysis on the two W-MB units with CuCrZr and RAFM-steel pipes showed acceptable under the steady-state heat loads of 10 and 5 MWm^{-2}, respectively.

K-DEMO divertor also consists of three plasma facing modules (inner target, dome and outer target) and CB as shown in Fig 12 (d) [21]. Hight of the dome structure is low, extending to the inner and outer reflectors. While the coolant routing was not proposed, thermal stress analysis on the W-MB units with CuCrZr and RAFM-steel pipes was performed under the steady-state peak heat load of 10 MWm^{-2} [65]. The former W-MB size was comparable to that of ITER and the latter was smaller, and the coolant conditions corresponded to 70 °C/4 MPa and 290 °C/15 MPa, respectively. The former showed similar result of ITER divertor target, i.e. maximum temperatures of the W-MB and CuCrZr pipe were ~1242 °C and ~271 °C. On the other hand, for the latter case, the maximum temperature reached a softening limit of the RAFM-steel (~550 °C) at the pipe top surface even though the pipe thickness was too thin (0.25 mm) for the higher pressurized coolant boundary. Design of the W-MB units and coolant routing is in progress.

4.3. Development of target technologies for DEMO

Mechanical property of the heat sink and thermal contact to joint/interlayer/W-MB are an important key issue for Cu-alloy application under neutron irradiation. Several technologies for

the high heat flux target have been developed in EU to survive under DEMO-relevant neutron irradiation condition. All are based on W-MB as a baseline plasma facing material, and Cu-alloy pipe with swirl tape to increase the heat transfer at the pipe wall [66, 67]. Material properties of CuCrZr and Cu-interlayer are anticipated to limit the performance of the target heat sink, e.g. irradiation creep above 350°C and irradiation embrittlement below 250°C [68]. Thus, it is reinforced by various kinds of Cu-W composite materials and novel interlayer materials as shown in Fig.16 [50].

(a) ITER-like W-MB with a CuCrZr pipe is a baseline concept also in the DEMO divertor, but the MB size is modified to decrease the crosssection width to 23 mm, instead of 28 mm in ITER in order to reduce thermal stresses and prevent vertical cracking. The axis thickness of 12 mm and thickness of 8 mm to the cooling pipe are the baseline design.

(b) Thermal break interlayer concept (developed in CCFC) is based on ITER W-MB target. The concept features cut-outs in the Cu-interlayer in the area of the highest heat flux to achieve a more uniform distribution of the thermal flux around the cooling pipe circumference.

(c) Composite pipe concept (developed in IPP) is based on a W wire-reinforced Cu composite pipe, which expects better strength of the cooling pipe, in particular, at high temperature (> 350 °C).

(d) Functionally graded W/Cu (FGM) interlayer concept (developed in CEA) aims replacing thick Cu interlayer, which is expected to be fully embrittled by fast neutron due to segregation of transmuted He at grain boundaries. Graded thin (20 μm) and think (500 μm) W-Cu interlayer is used to improve joining strength.

(e) Flat-tile concept with a composite heat sink block (developed in IPP): W particle-reinforced Cu composite block is expected to enhance the mechanical resilience of the irradiated heat sink against structure failure. The use of the W-Cu composite is supposed to reduce the thermal expansion mismatch between the armor tile and the heat sink block.

(f) In addition, He cooling target using multi-jet pipe by W and W-laminate (developed in KIT) is also developed as an option [66].

Recently, small-scale mock-ups of each concept have been fabricated and tested by means of hydrogen neutral beam in the GLADIS under the high power density at 20 MWm^{-2} up to 2000 cycles (130 °C coolant, which is expected operation temperature). A good production quality and reliable high-heat-flux fatigue performance was demonstrated. All mock-ups showed intact structural integrity and stable heat removal capacity over the entire loading cycles. Modest roughening of the W-MB surface and swelling of the blocks due to inelastic

deformation was found. The metallographic examination revealed that the upper half of the MBs were completely recrystalized, but no discernable cracks were found in any of the tested armor (290 blocks). Furthermore, other ITER-like mock-ups were tested at 25 MWm^{-2} up to 500 pulses (20°C and 100°C coolant conditions) for overload tests. Also under the increased heat load, the mock-ups exhibited intact structural integrity and stable heat removal capacity, even though there was a single fine crack (6 mm in depth) initiated from the MB surface which underwent a pronounced inelastic deformation leading to overall severe roughening. The mock-ups even withstood the overload up to 32 MWm^{-2} (5 pulses), which was the physical limit nearly reaching the melting temperature of the W-MB surface without any detrimental impact nor melting. The future R&D will be focused on an upscaling trial towards a medium-scale manufacturing (40 cm length).

5. Summary and future issues

Power exhaust concept and appropriate divertor design are common critical issues for DEMO design activities, which have been carried out in Europe, Japan, China, Korea and USA. At the same time, the divertor design is strongly affected by DEMO missions (net electricity generation, sufficient tritium breading and feasibility for remote maintenance) and design requirements from each DEMO concept. In this paper, conventional divertor concepts and power exhaust studies for recent DEMO designs (P_{fusion} = 1-2 GW, R_p = 7-9 m) were reviewed from the viewpoints of the plasma physics study and the divertor engineering design. Radiative cooling is a common approach for the power exhaust scenario, and water cooling divertor design with ITER-like target (W-PFC and Cu-alloy heat sink) is a common baseline. Some different design approaches have provided important case-studies of the DEMO divertor, and those will significantly contribute to future DEMO designs.

(1) Requirements of f_{rad}^{main} and plasma performance determine the divertor design concept:

Different power exhaust scenarios have been developed for DEMO concepts, while a common critical issue is the large power exhaust of P_{heat} = 280-600 MW in the main plasma and divertor by the radiative cooling ($P_{rad}^{tot}/P_{heat} \geq 0.8$). The steady-state plasma concepts such as JA DEMO and CFETR proposed a conventional closed divertor geometry to challenge large P_{sep}/R_p handling (25-30 MWm^{-1}) in order to maintain the ITER-level radiation fraction of the main plasma ($f_{rad}^{main} = P_{rad}^{main}/P_{heat}$ = 0.3-0.4) and higher plasma performance (HH_{98y2} =1.2-1.4). K-DEMO and FNSF will challenge larger P_{sep}/R_p handling (37-53 MWm^{-1}) with the

double null divertor configuration. The pulsed plasma concept (EU) challenges both increasing f_{rad}^{main} to ~0.65 and handling the ITER-level P_{sep}/R_p in *the open divertor geometry*, where increasing the tritium breading blanket volume is anticipated. These plasma concepts compromised requirements of increasing f_{rad}^{main} and high plasma performance ($HH_{98(y,2)}$, β_N, f_{BS}), which determined power handling in the divertor. In addition, adequate performance of the power exhaust will be required in the relatively low density plasmas. Design improvement is demanded from the viewpoints of reduction in the fuel dilution, and the power exhaust in the main plasma and divertor.

(2) Power exhaust simulations for DEMO divertor design (P_{sep} =150-300 MW) are in progress:

ITER-based divertor geometry (inclined target, baffle and dome structures) with longer leg length (1.6-1.7 m) is a common baseline design, and power exhaust simulations for DEMO divertor design with larger P_{sep} =150-300 MW have been performed using integrated divertor codes; SOLPS on EU DEMO and CFETR divertors, SONIC on JA DEMO divertor, UEDGE for K-DEMO and FNSF divertors. Divertor operation and influences of the key power exhaust parameters have been recently investigated with mainly Ar seeding, and all simulations showed reduction in the peak $q_{target} \leq 10 MWm^{-2}$ for the divertor radiation fraction (P_{rad}^{div}/P_{sep}) of 0.7-0.8. Some results were consistent with the design requirement for the n_e^{sep} range (JA: 2-3x10^{19}, EU: ~3x10^{19} m^{-3}) lower than that of ITER. Comparisons showed benefit of the closed geometry to reduce the peak q_{target} and T_e^{div} near the separatrix. All results also suggested that partial detachment was expected in the outer divertor for the vertical target geometry, and that the peak q_{target} location and value (and each heat load component) significantly changed in the attached or detached region. In addition, uncertainty of high T_e^{div} and T_i^{div} in attached region (far-SOL) was a critical issue for plasma/impurity transport and tungsten (W) erosion. Further improvements of the divertor geometry and operation options such as different seeding impurity will be explored in order to extend the detachment width and to reduce local T_e^{div} and T_i^{div} at the attached plasma region.

Diffusion coefficients of heat and particle fluxes (χ and D) are a critical for DEMO divertor design and operation. Different values and/or profiles were so far applied to produce $\lambda_{q//}$ =2-3 mm near the separatrix in SOL, which was slightly smaller than that of ITER due to high T_e and T_i under the DEMO SOL condition. While the large heat flux ($q_{//}$) near the separatrix could be reduced along the long leg in the divertor, reduction in χ and D significantly affected the divertor power exhaust over the whole SOL region due to increase of the $q_{//i}$ profile as well as

the dominant $q_{//e}$ near the separatrix. Feasible values or profile of the diffusion coefficient over the near- and far-SOLs will be also demanded in order to determine the divertor operation for the DEMO design.

SOLPS-ITER simulation results with various drifts activated showed that inboard-enhanced asymmetry of the particle flux profile and outboard-enhanced heat load profile were produced even in the long-leg divertors of EU DEMO and CFETR. The latter recently proposed to further extend the divertor leg in order to insure the detached divertor operation window at lower n_e^{sep}. Other physics factors to modify the DEMO divertor design such as dissipations in the high density divertor (charge exchange, photon absorption and collisional-radiative models) and kinetic effects in low collisionality SOL (flux limiter, thermal force) were also pointed out.

(3) A common baseline design for DEMO divertor, and specific design and R&D issues:

Integrated designs of the water cooled divertor target, cassette and cooling pipe routing have been also developed, based on the ITER W monoblock (MB) concept with Cu-alloy pipe. Engineering design adequate under higher neutron irradiation condition is required. Selection and arrangement of the divertor plasma facing unit, coolant condition and routing for recent design concepts of EU DEMO, JA DEMO, CFETR and K-DEMO were summarized. Under a year-long and DEMO-level neutron irradiation condition, mechanical property of the CuCrZr heat sink and the Cu interlayer was anticipated to be induced embrittlement, thus the coolant temperature (T_{cool}) for the high heat flux component was increased to higher than that of ITER (~70 ℃). The inlet-T_{cool} was so far selected to be large variation between 70 ℃ and 200 ℃ (K-DEMO: 70 ℃, EU DEMO: 130 ℃, CFETR: 140-180 ℃, JA DEMO: 200 ℃). At the same time, influence of thermal softening on the CuCrZr pipe was fostered near the strike-point when the high heat load of 10 MWm^{-2}-level was exposed. DEMO specific risks such as neutron induced embrittlement/softening of the interlayers and cooling pipe have been recognized and further restrictions of q_{target}, T_e^{div} and surface temperature were anticipated. Improved technologies of high heat flux components based on the ITER W-MB unit have been developed in EU in order to reduce thermal stress and to strengthen the heat sink and interlayer under higher irradiation dose condition.

Recent integrated design of the divertor target, CB and coolant pipe routing were also shortly reviewed. Two coolant conditions (lower- and higher-T_{cool}) for the Cu-alloy and RAFM steel heat sink MB units, respectively, where the latter coolant also used for CB and supporting structures. Appropriate conditions for the latter coolant, i.e. 180-200 °C/ 5 MPa (EU-DEMO)

and 290 °C/15 MPa (JA DEMO, CFETR and K-DEMO), will be determined in the future optimization of the divertor and DEMO design concept. In addition, a common issue of series or parallel coolant pipe routing for the DEMO divertor design was compared.

Acknowledgments

Authors thank Y. Homma(QST), H. Utoh(QST), Y. Somaya(QST), S. Yamoto (QST), Y. Sakamoto（QST）, M. Tokitani (NIFS) and Joint Special Design Team for Fusion DEMO (Japan), M. Siccinio (IPP, Garching), G. Mazzone (ENEA), D. Marzullo (Univ. Trieste), S. Roccella (ENEA), H. Greuner (MPG), C. Kessel (ORNL), S.-H. Hong (GA) for giving useful information and comments. First author thanks continuous support by Japan and Europe home teams (QST in Rokkasho, and EUROfusion Programme Management Unit in Garching), and DEMO Design Activity (DDA) unit of the IFERC project team.

SONIC simulations were carried out within the framework of the Broader Approach DEMO Design Activity, using the JFRS-1 supercomputer system at CSC, IFERC, Rokkasho, Japan.

The contributions of T.D. Rognlien was supported by the US Department of Energy under DE-AC52-07NA27344 at LLNL.

References

[1] R. Wenninger, et al., The physics and technology basis entering European system code studies for DEMO, Nucl. Fusion **57** (2017) 016011.

[2] G. Federici, et al., DEMO design activity in Europe: Progress and updates, Fusion Eng. Des. **136** (2018) 729.

[3] Y. Sakamoto, et al., DEMO Concept Development and Assessment of Relevant Technologies, 25th IAEA Int. Conf. on Fusion Energy (St. Petersburg, Russia, 2014) FIP/3-2Rb.

[4] K. Tobita, et al., Design Strategy and Recent Design Activity on Japan's DEMO, Fusion Sci. Technol. **72** (2017) 537.

[5] G. Zhuang, et al., Progress of the CFETR design, Nucl. Fusion **59** (2019) 112010.

[6] K. Kim, et al., Design of K-DEMO for near-term implementation, Nucl. Fusion **55** (2015) 053027.

[7] J.S. Kang, et al., Development of a systematic, self-consistent algorithm for the K-DEMO steady-state operation scenario, Nucl. Fusion **57** (2017) 126034.

[8] C. E. Kessel, et al., Core plasma physics basis and its impacts on the FNSF, Fusion Eng. Des. **135** (2018) 356-369.

[9] M. Shimada, et al., Chapter 1: Overview and summary, Nucl. Fusion **47** (2007) S01.

[10] A. Loarte, et al., Chapter 4: Power and particle control, Nucl. Fusion **47** (2007) S203.

[11] G. Federici, et al., Overview of the DEMO staged design approach in Europe, Nucl. Fusion 59 (2019) 066013.

[12] C. E. Kessel, et al., The ARIES Advanced and Conservative Tokamak Power Plant Study, Fusion Sci. Technol. **67** (2015) 1.

[13] N. Asakura, et al., Simulation studies of divertor detachment and critical power exhaust parameters for Japanese DEMO design, Nucl. Meter. Energy **26** (2021) 100864.

[14] N. Asakura, et al., Development and Application of SONIC Divertor Simulation Code to Power Exhaust Design of Japanese DEMO Divertor, Processes **10** (2022) 872.

[15] F. Subba, et al., Modelling of mitigation of the power divertor loading for the EU DEMO through Ar injection, Plasma Phys. Control. Fusion **60** (2018) 035013.

[16] F. Subba, et al., SOLPS-ITER modeling of divertor scenarios for EU-DEMO, Nucl. Fusion **61** (2021) 106013.

[17] N. Asakura, et al., Power Exhaust Concepts and Divertor Designs for Japanese and European DEMO Fusion Reactors. Nucl. Fusion **61** (2021) 126057.

[18] L. Aho-Mantila, et al., Predictions of radiation pattern and in–out asymmetries in the DEMO scrape-off layer using fluid neutrals, Nucl. Fusion **62** (2022) 056015.

[19] X. J. Liu, et al., Simulation studies of divertor power exhaust with neon seeding for CFETR with GW-level fusion power, Phys. Plasmas **27** (2020) 092508.

[20] H. Si, et al., SOLPS-ITER simulations of high power exhaust for CFETR divertor with full drifts, Nucl. Fusion **62** (2022) 026031.

[21] S. Kwon, et al., Recent progress in the design of the K-DEMO divertor, Fusion Eng. Des. **159** (2020) 111770.

[22] T.D. Rognliena, et al., Scrape-off layer plasma and neutral characteristics and their interactions with walls for FNSF, Fusion Eng. Des. **135** (2018) 380–393.

[23] M. E. Rensink, et al., Plasma Heat-Flux Dispersal for ACT1 Divertor Configurations, Fusion Sci. Technol. **67** (2015) 125-141.

[24] R. A. Pitts, et al., Physics basis for the first ITER tungsten divertor, Nucl. Meter. Energy **20** (2019) 100696.

[25] R. A. Pitts, et al., A full tungsten divertor for ITER: Physics issues and design status, J. Nucl. Mater. **438** (2013) S48.

[26] M. Siccinio, et al., Figure of merit for divertor protection in the preliminary design of the EU-DEMO reactor, Nucl. Fusion **59** (2019) 106026.

[27] N. Asakura, et al., Studies of power exhaust and divertor design for a 1.5 GW-level fusion power DEMO, Nucl. Fusion **57** (2017) 126050.

[28] M. Kovari, et al., PROCESS: A systems code for fusion power plants–Part 2: Engineering, Fusion Eng. Des. **104** (2016) 9.

[29] M. Nakamura, et al., Efforts towards improvement of systems codes for the Broader Approach DEMO design, Fusion Eng. Des. **87** (2012) 864.

[30] Y.R. Martin, et al, Power requirement for accessing the H-mode in ITER, J. Phys.: Conf. Ser. **123** (2008) 012033.

[31] M. Siccinio et al., Figure of merit for divertor protection in the preliminary design of the EU-DEMO reactor, Nucl. Fusion **59** (2019) 106026.

[32] A. Kallenbach, et al., Optimized tokamak power exhaust with double radiative feedback in ASDEX Upgrade, Nucl. Fusion **52** (2012) 122003.

[33] A. Kallenbach, et al., Partial detachment of high power discharges in ASDEX Upgrade, Nucl. Fusion **55** (2015) 053026.

[34] N. Asakura, et al., Investigations of impurity seeding and radiation control for long-pulse and high-density H-mode plasmas in JT-60U, Nucl. Fusion **49** (2009) 115010.

[35] H. Utoh, et al., Studies of the Plasma Vertical Instability and its Control Concepts in JA and EU Broader Approach, DEMO Design Activity, Fusion Eng. Des. **136** (2018) 874.

[36] A. Huber, et al., Comparative H-mode density limit studies in JET and AUG, Nucl. Metter. Energy **12** (2017) 100.

[37] A. Kukushkin, et al., Consequences of a reduction of the upstream power SOL width in ITER. J. Nucl. Mater. **438** (2013) S203-S207.

[38] T. Eich, et al., Scaling of the tokamak near the scrape-off layer H-mode power width and implications for ITER. Nucl. Fusion **53** (2013) 093031.

[39] A. Kallenbach, et al., Multi-machine comparisons of H-mode separatrix densities and edge profile behaviour in the ITPA SOL and Divertor Physics Topical Group. J. Nucl. Mater **337** (2005) 381-385.

[40] A.W. Leonard, et al., Compatibility of separatrix density scaling for divertor detachment with H-mode pedestal operation in DIII-D. Nucl. Fusion **57** (2017,) 086033.

[41] T. Eich, et al., JET Contributors; Correlation of the tokamak H-mode density limit with ballooning stability at the separatrix. Nucl. Fusion **58** (2018) 034001.

[42]A. Loarte, Effects of divertor geometry on tokamak plasmas, Plasma Phys. Control. Fusion **43** (2001) R183–R224.

[43] S. Qin, et al., Design analysis and remote handling compatibility for a CFETR long leg divertor concept, Fusion Eng. Des. **167** (2021) 112351.

[44] D. Reiter, The TRIM code surface database (http://eirene.de/trim.pdf) (2010).

[45] A. V. Chankin, et al., Monte Carlo simulations of tungsten redeposition at the divertor target, Plasma Phys. Control. Fusion **56** (2014) 025003.

[46] A. Kallenbach, et al., Partial detachment of high power discharges in ASDEX Upgrade, Nucl. Fusion **55** (2015) 053026.

[47] F. Maviglia, et al., Limitations of transient power loads on DEMO and analysis of mitigation techniques, Fusion Eng. Des. **109–111B** (2016) 1067-1071.

[48] S.I. Krasheninnikov, Reverse flow and parameter profiles in a dense tokamak divertor plasma. Nucl. Fusion **32** (1992) 1927-1934.

[49] G. Mazzone, et al., Eurofusion-DEMO Divertor - Cassette Design and Integration, Fusion Eng. Des. **157** (2020) 111656.

[50] J.H. You, et al., Divertor of the European DEMO: Engineering and technologies for power exhaust, Fusion Eng. Des. **175** (2022) 113010.

[51] X.Y. Qian, et al., New designs of target and cooling scheme for water cooled divertor in DEMO, Nucl. Fusion **61** (2021) 036008.

[52] R. Villari, et al., Nuclear analysis of the ITER full-tungsten divertor, Fusion Eng. Des. **88** (2013) 2006.

[53] A. Hasegawa, et al., Neutron irradiation effects on tungsten materials, J. Nucl. Mater. **89** (2014) 1568-1572.

[54] Y. Ueda, et al., Baseline high heat flux and plasma facing materials for fusion, Nucl. Fusion **57** (2017) 092006.

[55] Ch. Linsmeier, et al., Development of advanced high heat flux and plasma-facing materials, Nucl. Fusion **57** (2017) 092007.

[56] A. Alfonso et al., Recrystallization kinetics of warm-rolled tungsten in the temperature range 1150–1350 °C, J. Nucl. Mater. **455** (2014) 591.

[57] A. Alfonso, et al., Thermal stability of a highly-deformed warm-rolled tungsten plate inthe temperature range 1100–1250°C, Fus. Eng. Des. **98-99** (2015) 1924.

[58] M. Tokitani, et al., Application of the advanced multi-step brazing for fabrication of the high heat flux component J. Nucl. Mater. **538** (2020) 152264.

[59] S.A. Fabritsiev, et al., Evaluation of copper alloys for fusion reactor divertor and first wall components, J. Nucl. Mater. **233–7** (1996) 127–37.

[60] S.A. Fabritsiev, et al., Effect of high doses of neutron irradiation on physicomechanical properties of copper alloys for ITER applications, Fusion Eng. Des. **73** (2005) 19–34.

[61] J.-H. You, et al., A review on two previous divertor target concepts for DEMO: mutual impact between structural design requirements and materials performance Nucl. Fusion **55** (2015) 113026.

[62] Y. Someya, et al., Design study of blanket structure based on a water-cooled solid breeder for DEMO, Fusion Eng. Des. **98–99** (2015) 1872.

[63] J.-H. You, et al., Structural lifetime assessment for the DEMO divertor targets: Design-by-analysis approach and outstanding issues, Fusion Eng. Des. **164** (2021) 112203.

[64] M. Fursdona, J-H. You, Towards reliable design-by-analysis for divertor plasma facing components—Guidelines for inelastic assessment (part II: irradiated), Fusion Eng. Des. **160** (2020) 111831.

[65] S. Kwon, et al., Thermo-hydraulic optimization study for a high heat flux unit of the K-DEMO divertor target, Fusion Eng. Des. **134** (2018) 68–73.

[66] J.H. You, et al., European divertor target concepts for DEMO: Design rationales and high heat flux performance, Nucl. Mater. Energy **16** (2018) 1.

[67] J.H. You, et al., High-heat-flux technologies for the European demo divertor targets: State-of-the-art and a review of the latest testing campaign, J. Nucl. Mater. **544** (2021) 152670.

[68] J.H. You, et al., A review on two previous divertor target concepts for DEMO: mutual impact between structural design requirements and materials performance, Nucl. Fusion **55** (2015) 113026.

Tables

Table 1 Key design parameters of recent DEMO concepts, obtained by system codes.

Parameters	EU DEMO [1,2]	JA DEMO 2014 [3,4]	CFETR (1st stage)[5]	K-DEMO (1st phase) [6,7]	FNSF [8]	ITER (inductive, Q=10)[9,10]
R_p (m)/ a_p (m)	9.0/ 2.9	8.5/ 2.4	7.2/ 2.2	6.8/ 2.1	4.8/ 1.2	6.2/ 2.0
A	3.1	3.5	3.3	3.2	3.5	3.1
I_p (MA)	18.0	12.3	13.8	12.3	7.9	14
B_T (T)/ B_T^{max} (T)	5.9/ 12.5	5.94/ 12.1	6.5/ 14	7.4/ 16	7.5/ 15.9	5.3/ 12
κ_{95}	1.6	1.65	2.0	1.8	2.1	1.7
q_{95}	3.5	4.1	5.5	7.3	6.0	3
Operation	Pulsed 2-hours	steady-state	steady-state	steady-state	steady-state	~400s
Divertor configuration	Single null (option: Double null)	Single null	Single null	Double null	Double null	Single null
P_{fusion} (MW)	2000	1462	974	2200	520	500
P_{aux} (MW)	50	84	82	160	129	73 (installed)
P_{heat}: P_α+P_{aux} (MW)	457	376	277	600	233	~150
P_{heat}/R_p (MWm^{-1})	53	44	39	88	49	24
ave. neutron load to first wall (MWm^{-2})	~1	~1	~0.7	~2	~1.2	0.5

Table 2 Power exhaust parameters of DEMO concepts with the single null divertor

Parameters	EU DEMO1 [1]	JA DEMO higher-κ [27]	CFETR steady-state [19]
line-ave. n_e (10^{19}m^{-3})	8.7	8.6	6.3
n^{GW} (10^{19} m^{-3})	7.2	7.3	9.1
line-ave. n_e/n^{GW}	1.2	1.2	0.67
Seeding (n_{imp}/n_e, %)	Xe (0.039)+Ar	Ar (0.6)	Ar/Ne
P_{heat} (MW)	457	435	305
P_{rad}^{main} (MW)	306	177	86
P_{rad}^{main}/P_{heat}	0.67	0.41	0.28
P_{sep} (MW)	154	258	219
P_{sep}/R_p(MWm^{-1})	17	30	28
P_{LH} in DT(MW)	133	115	68
$f_{LH} = P_{sep}/P_{LH}$	1.2	2.2	3.2

Table 3 Power exhaust and diffusion coefficients of DEMO divertor simulation

Parameters	EU DEMO [16]	JA DEMO [13,27]	CFETR [19]	FNSF[22]
Divertor code	SOLPS-ITER	SONIC	SOLPS5.0	UEDGE
P_{sep} (MW)	~146	~235	~193	~88 (lower divertor)
T_e^{sep} (keV)	0.2	0.37	0.46	~0.2
T_i^{sep} (keV)	0.5	0.83	2.1	~0.5
n_e^{sep} (10^{19} m^{-3})	2.8	2.0	1.7	~6
$\chi^{edge/SOL}$ (m^2 s^{-1})	0.2/ 0.18	1.0	1.0	0.5
$D^{edge/SOL}$ (m^2 s^{-1})	0.2/ 0.42	0.3	0.3	0.33
$\lambda_{q//}^{mid}$ (mm)	~3	2.9	~3	~2

Table 4 Estimation of W erosion depth at the peak T_e^{div} by seeding impurities

	EU DEMO [16]	JA DEMO [13,27]	CFETR [19]	FNSF[22]
T_e^{div} *at* r^{div} (attached region)	20 eV at 40cm	25 eV at 20cm	20 eV at 45cm	40 eV at 45cm
Γ_i^{div} ($m^{-2}s^{-1}$)	~10^{21}	4x10^{22}	5x10^{21}	~10^{22}
$c_Z = n_Z/n_i$ (%)	1 (Ar)	0.4 (Ar)	0.6 (Ne)	0.4 (Ne)
$Y_Z * c_Z * \Gamma_i^{div}$ ($m^{-2}s^{-1}$)	6.3x10^{17} (*1)	1.9x10^{19}	8x10^{19}	7x10^{18}
Net erosion ratio: R_{net}	0.1	0.1	0.03	0.1 (*2)
Δd_{sec} (nm s^{-1})	~0.001	0.03	0.04	0.011
Δd_{year} (mm $year^{-1}$)	~0.03	~0.9	~1.2	~0.3

Note *1: calculation is performed using the TRIM database [44].

Note *2: prompt re-deposition reduction factor is chosen from [45].

Table 5 Key components and parameters of armor, heat sink and cassette for water-cooling divertor concepts of EU DEMO, JA DEMO, CFETR and K-DEMO.

		EU DEMO1 [49,50]	JA DEMO [17]	CFETR(1st stage) [43,51]	K-DEMO [21,52]
Number of cassette		48	48	80	32 (upper/lower)
Number of divertor maintenance ports		16	16	16	16
Total cassette weight incl. PFC units (ton)		8.3	~22	~8	TBD
Target	Plasma facing component	W	W	W	W
	Heat sink pipe	CuCrZr	CuCrZr	CuCrZr	CuCrZr/RAFM-steel
	Water temperature (℃)/ P(MPa)	130/ 5	200/ 5	140-180/ 5	70/4 or 290/15
	Dose on PFC (dpa·FPY^{-1})	< 1.9	< 0.5	< 0.5	< 0.4
	Dose on cooling pipe (dpa·FPY^{-1})	< 7.2	< 1.5	< 1.5	<1.9 or <1.2
Upper target (Baffle)	Plasma facing component	---	W	W	W
	Heat sink pipe	---	F82H	CuCrZr/RAFM-steel	RAFM-steel
	Water temperature (℃)/ Pressure (MPa)	---	290/ 15	140-180/ 5	150/ 5
	Dose on PFC (dpa·FPY^{-1})	---	< 2	< 2	< 2.6
	Dose on cooling pipe (dpa·FPY^{-1})	---	< 6	< 6	< 10.9
Dome (Liner)	Plasma facing component	W (*1)	W	W	W
	Heat sink pipe	EUROFER97	F82H	CuCrZr/RAFM-steel	RAFM-steel
	Water temperature (℃)/ Pressure (MPa)	180/ 3.5	290/ 15	140-180/ 5	150/ 5
	Dose on PFC (dpa·FPY^{-1})	<1.8	< 1.6	< 2	< 1.9
	Dose on cooling pipe (dpa·FPY^{-1})	<5	< 5	< 6	< 7.8
Cassette	Structural material	EUROFER97	F82H	SS316L/RAFM-steel	RAFM-steel
	Water temperature (℃)/ Pressure (MPa)	180/ 3.5	290/ 15	140-180/ 5	290/ 15
	Dose on structural material (dpa·FPY^{-1})	< 6	< 3	TBD	TBD

Note *1) Baffle is not installed. Liner is installed for protection against the plasma and neutron irradiation.

Table 6 Design constrains of Cu and Cu-alloy under neutron irradiation condition [17]

		Softening			Embrittlement	Thermal cond.reduction
Heat sink/ Coolant pipe	Yield strength at RT (MPa)	Threshold (˚C)	Radiation-induced (dpa)		Embrittlement by transmuted He (dpa)	Reduction (20%) by transmuted product (dpa)
			hardening	softening		
Cu	~60 MPa	---	~0.1	---	6 (at 350˚C) 40 appm limit with 7appm/dpa	10
CuCrZr	>400 MPa	280	~0.2	~1		10
ODS-Cu(GlidCop[58])	>400 MPa	300	~0.2	1~2		10

Figure captions

Figure 1

Constant lines of $P_{sep}B_T/q_{95}R_pA$ ~9 MWTm^{-1}, $\hat{c}_{Z,det} \leq 1$ and $f_{LH} = 1$ in the f_{LH} - R plane (a) and $f_{LH} - B_T$ plane (b) for EU DEMO1 study, assuming $P_{fusion} = 2$ GW. The reference design point is represented with a red point ($R_p = 9.0$m, $B_T = 6$T, $f_{LH} = 1.2$). Green shaded areas "A" identify the feasible EU-DEMO configurations, the red shaded areas "B" identify the configuration which would be feasible if advanced superconducting magnetic technology (a higher magnetic field in a smaller space than current one) is provided. [29] (c) P_{fusion}, P_{rad}^{main}, P_{sep} as a function of Ar impurity concentration ($c_{Ar} = n_{Ar}/n_e$) for JA DEMO with increasing $\kappa_{95} = 1.75$. $HH_{98(y,2)}$ required for $\beta_N = 3.4$ is increased with increasing c_{Ar}. Design point of JA DEMO higher-κ is shown in large circles ($c_{Ar} = 0.6\%$). Power handling parameter for the divertor (P_{sep}/R_p) is also shown.[25]

Figure 2

Fraction of P_{rad}^{main} in the total heating power (P_{heat}) and the divertor power handling (P_{sep}/R_p) for ITER, EU DEMOs (DEMO1, Flexi-DEMO), JA DEMOs (DEMO 2014, DEMO higher-κ) and CFETR (hybrid and steady-state concepts). Results of impurity seeding experiments in AUG[31] and JT-60U[32] are also shown by squares and circles: orange and green colors correspond to attached and detached divertor cases.

Figure 3

(a) SONIC simulation mesh and the divertor geometry of JA DEMO [13]. (b) SOLPS5.0 simulation mesh and the divertor geometry of CFETR [28]. (c) SOLPS-ITER simulation mesh and the divertor geometry of EU DEMO [16].

Figure 4

(a)(b) Distributions of Ar radiation power density (W_{rad}) in the inner and outer divertors, respectively: $n_e^{sep} = 2.0 \times 10^{19}$m^{-3}, $P_{out} = 250$ MW, $P_{rad}^{edge} + P_{rad}^{sol} + P_{rad}^{div} = 200$ MW and P_{sep} =235 MW. Profiles of (c) (d) n_e^{div}, T_e^{div} and T_i^{div}, (e)(f) integrating heat load components at the inner and outer divertor target, respectively [13].

Figure 5

Four series of peak q_{target} at the outer target for given exhaust power (P_{sep}) and radiation fraction in the SOL and divertor ($f^*_{rad}{}^{div} = (P_{rad}{}^{sol}+P_{rad}{}^{div})/P_{sep}$) as a function of $n_e{}^{sep}$ [13]. Circles and squares show Case-1; JA DEMO higher-κ reference (P_{sep} ~235MW, $f^*_{rad}{}^{div}$ ~0.8) and Case-2; JA DEMO 2014 reference (P_{sep} ~283MW, the same $f^*_{rad}{}^{div}$). Triangles and diamonds show Case-3 and Case-4, respectively, i.e. lower $f^*_{rad}{}^{div}$ (~0.7) cases corresponding to Case-1 and Case-2.

Figure 6

(a) Distribution of line radiation power density in the divertor for EU DEMO simulation. Profiles of (b) (d) $n_e{}^{div}$ and $T_e{}^{div}$, (c)(e) integrating heat load components at the inner and outer divertor target, respectively [16]. Radial coordinate for the heat load profiles (c)(e) is shifted to correspond to the plasma profiles (b) (d). Vertical dotted lines corresponding the heat load peak locations.

Figure 7

Vertical bars show radiation power fractions in the different plasma regions in inner SOL+divertor, outer SOL+divertor, private flux, and core (between core-edge boundary and separatrix) regions, as a function of Ar seeding rate. Dotted lines show total radiation fractions of $(P_{rad}{}^{edge}+P_{rad}{}^{sol}+P_{rad}{}^{div})/P_{out}$ and $(P_{rad}{}^{sol}+P_{rad}{}^{div})/P_{out}$. [18]

Figure 8

UEDGE calculation mesh for a baseline divertor design (vertical target geometry; $\theta^{tiv} = 25°$), and other open target geometries ($\theta^{tiv} = 40°$ and $70°$). Baseline design result: (b) The total heat load along the outer divertor plate, (c) Heat load components of radiation, electron heat flux, ion and neutral heat flux including charge exchange and recombination processes, and surface recombination, (d) profiles of electron density and temperature. Open target case ($\theta^{tiv} = 70°$): (e) Total heat load along the outer divertor plate, and heat load components of electron and ion heat fluxes, and surface recombination.

Figure 9

(a)Maximum T_e at the attached region of the outer target, and corresponding T_e near the separatrix at the midplane. (b) Ar concentration near the separatrix at the midplane SOL as a function of $n_e{}^{sep}$. Circles, squares and triangles correspond to Case-1, Case-2 and Case-3,

respectively.

Figure 10

Electron, ion and total parallel heat flux profiles ($q_{//e}^{Xp}$, $q_{//i}^{Xp}$, $q_{//e}^{Xp} + q_{//i}^{Xp}$) in the outer SOL near the X-point; (a) standard χ and D case (1.0 and 0.3 m^2s^{-1}) and (c) smaller case (0.5 and 0.15 m^2s^{-1}). Mach number profiles of the parallel plasma flow in SOL; (b) and (d), respectively. Distance from the separatrix near the X-point is mapped to the midplane SOL radius.[14]

Figure 11

Representative peak q_{target} at the outer target for four series of P_{sep} (~235/283 MW) and $f^*_{rad}{}^{div}$ (~0.67/0.78) as a function of n_e^{sep} [13]. Open symbols show corresponding four results with reducing $\chi_e = \chi_i = 0.5$ m^2s^{-1} and $D = 0.15$ m^2s^{-1}. Four guidelines correspond to results with standard χ and D.

Figure 12

Recent divertor designs for (a) EU DEMO [50], (b) JA DEMO [17], (c) CFETR [51], (d) K-DEMO [21].

Figure 13

Design of JA DEMO divertor (2020): (a) arrangement of the targets, baffles, reflectors, dome and cooling pipes in a cassette, (b) flow velocity, coolant temperature and pressure in the CuCrZr and F82H pipes for the heat sink units. Here, heat removal is evaluated with assuming both the inner and outer q_{target} to be 10 MWm^{-2}, which was larger than the simulation result in Sec. 3.2. [17]

Figure 14

Recent design of EU DEMO divertor (2019) [50]: (a) cassette with target plates, shielding liner and cooling manifold, higher temperature (180-210 °C) coolant route is shown by arrows. (b) Arrows show lower temperature (130-140 °C) coolant route for inner and outer targets. (c) Flow velocity, coolant temperature, pressure for targets and cassette body.

Figure 15

(a) Early divertor concept of CFETR divertor design [43]: the divertor consists of three first

wall modules (inner target, dome and outer target) and cassette body. The water route in the divertor cassette is toroidally divided to left- and right-sides. (b) Hybrid coolant cooling circuit [51]; OVT: outer target and baffle; IVT: inner target and baffle; Dome: umbrella, inner and outer reflector plates. The number is the quantity of the cooling unit channels. (c) schematic of streaming sequence of the coolant. Dome part I and II describe Dome module divided toroidally.

Figure 16

High heat flux target technologies developed for EU DEMO divertor [50]: (a) ITER-like monoblock baseline concept, (b) thermal break interlayer concept, (c) composite pipe of W-wire in Cu (Wf/Cu), (d) graded interlayer, (e) Flat W-tiles and W particle/Cu composite block.

Figures

Figure 1 (2 columns)

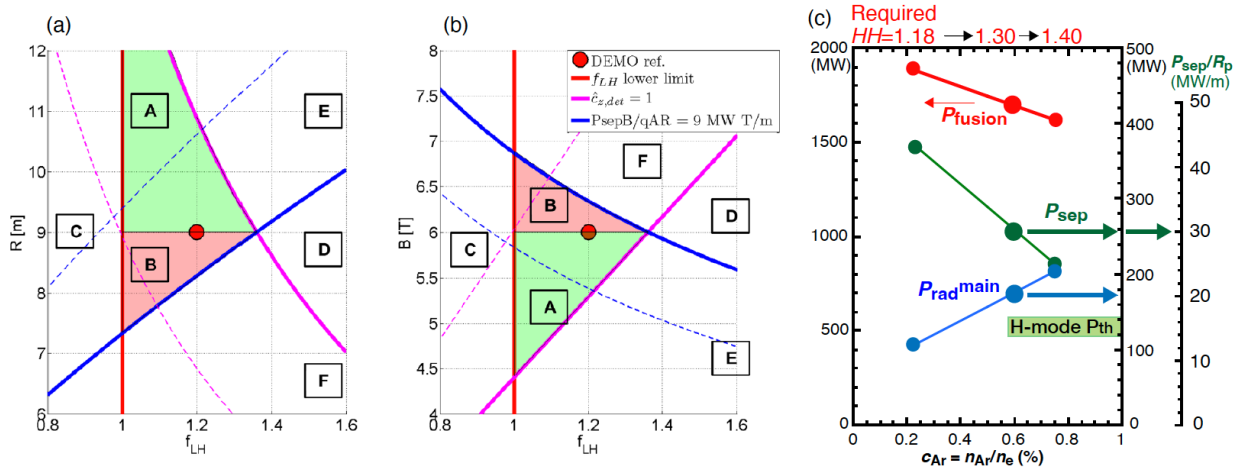

Figure 2 (1 column)

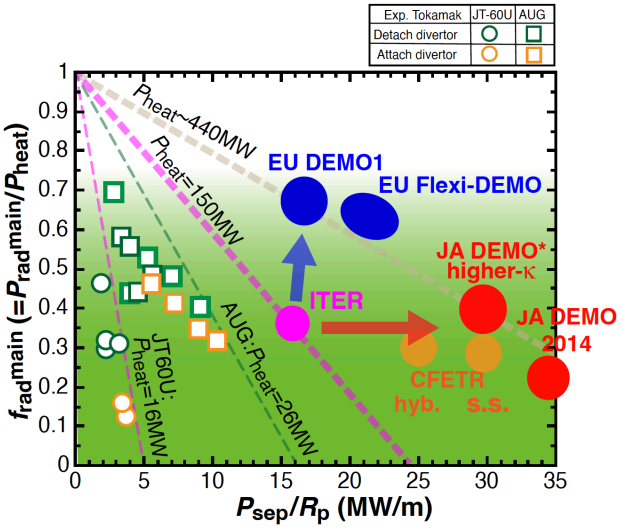

Figure 3 (2 columns)

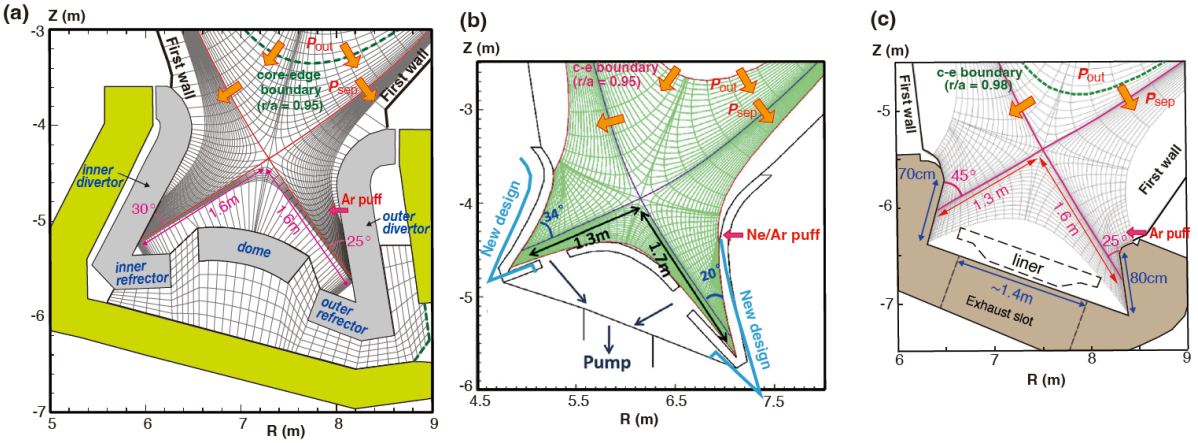

Figure 4 (2 columns)

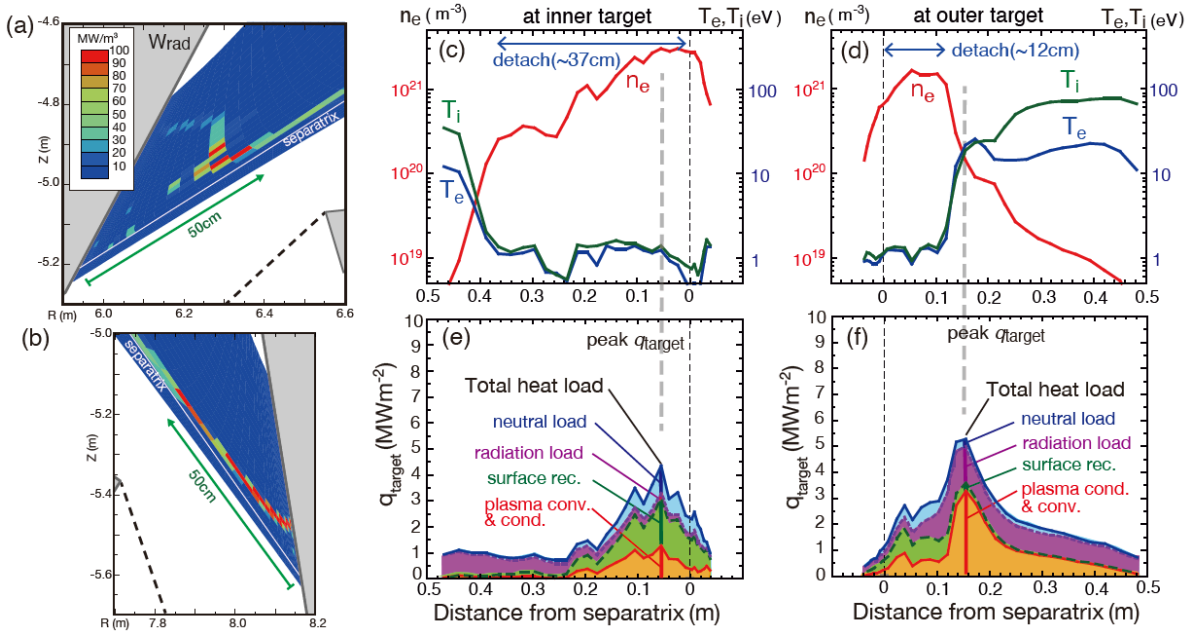

Figure 5 (1 column)

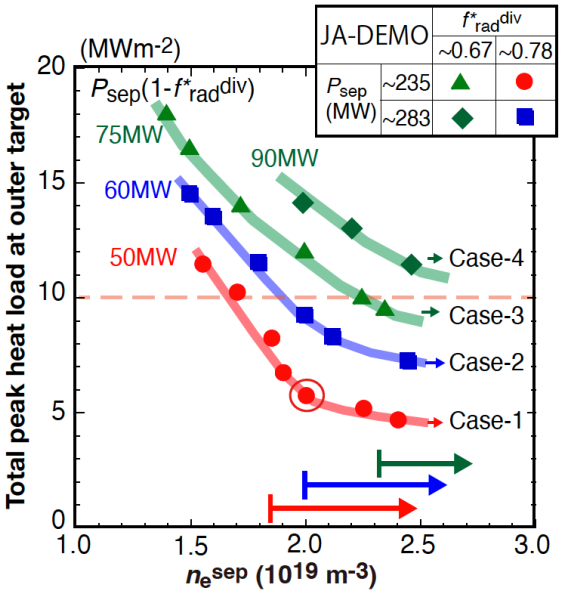
JA-DEMO
$f^*_{rad}{}^{div}$
~0.67
~0.78
P_{sep} (MW)
~235
~283
(MWm-2)
$P_{sep}(1-f^*_{rad}{}^{div})$
75MW
90MW
60MW
50MW
Case-4
Case-3
Case-2
Case-1
Total peak heat load at outer target
n_e^{sep} (10^{19} m^{-3})
20
15
10
5
0
1.0
1.5
2.0
2.5
3.0

Figure 6 (2 column)

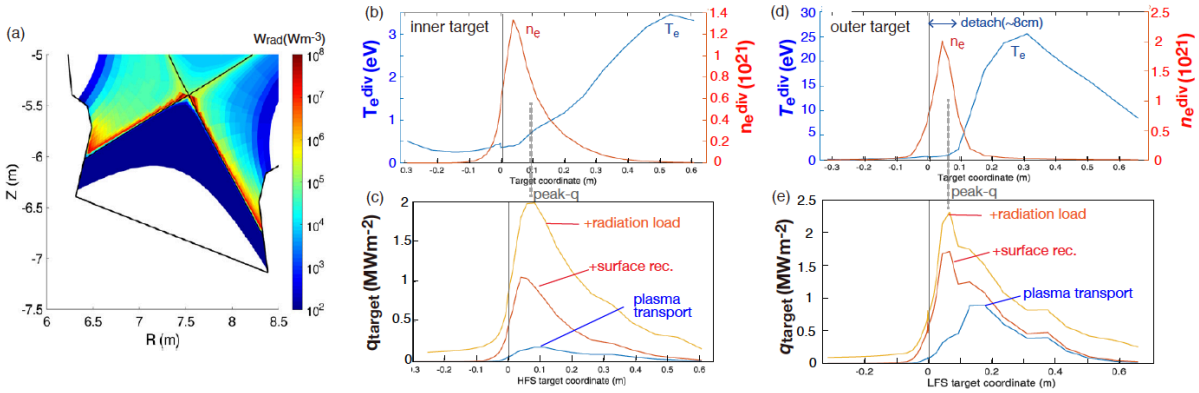

Figure 7 (1 column)

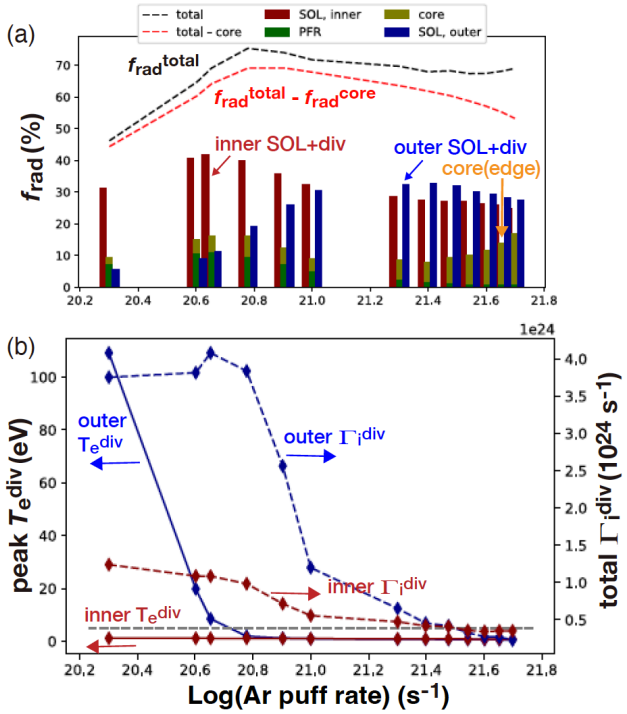

Figure 8 (2 columns)

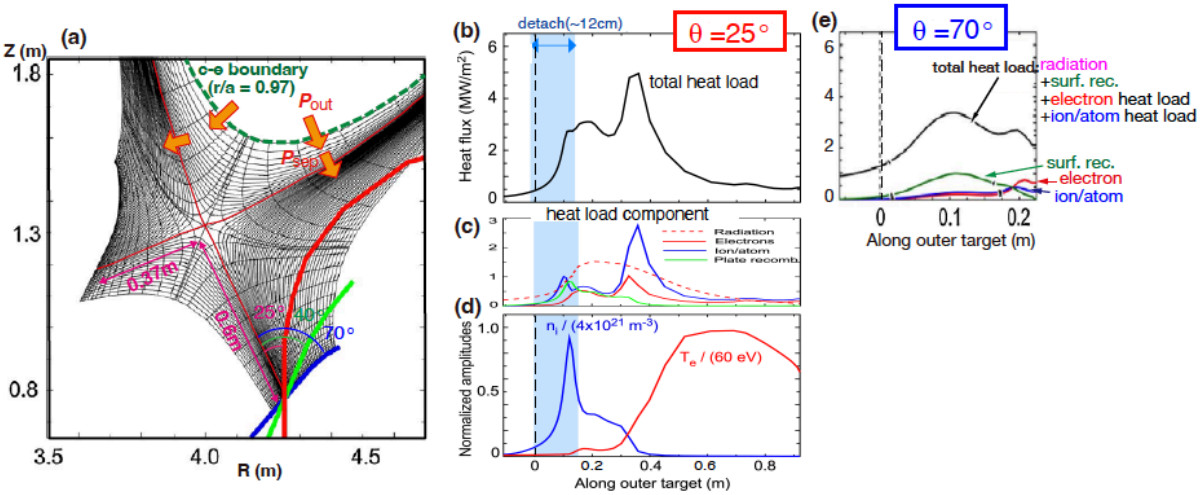

Figure 9 (2 columns)

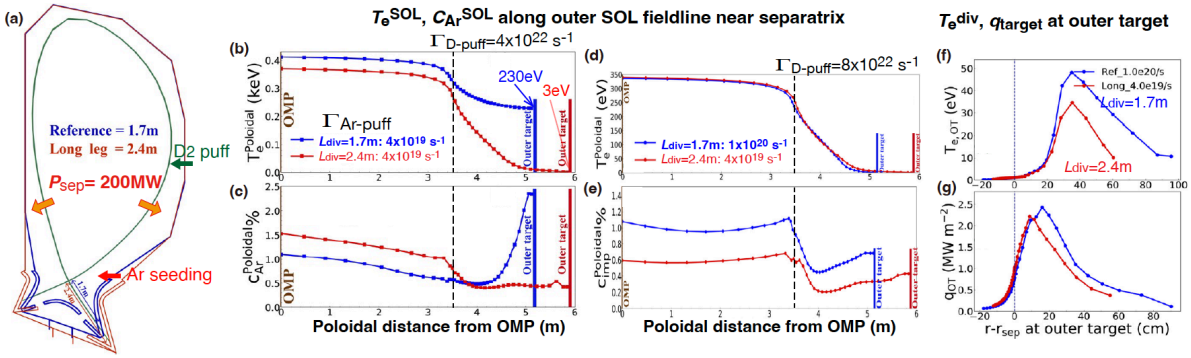

Figure 10 (1 column)

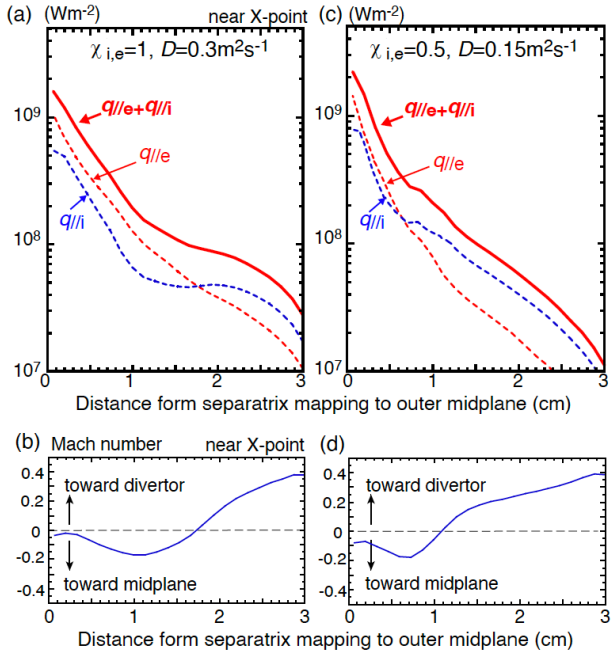

Figure 11 (1 column)

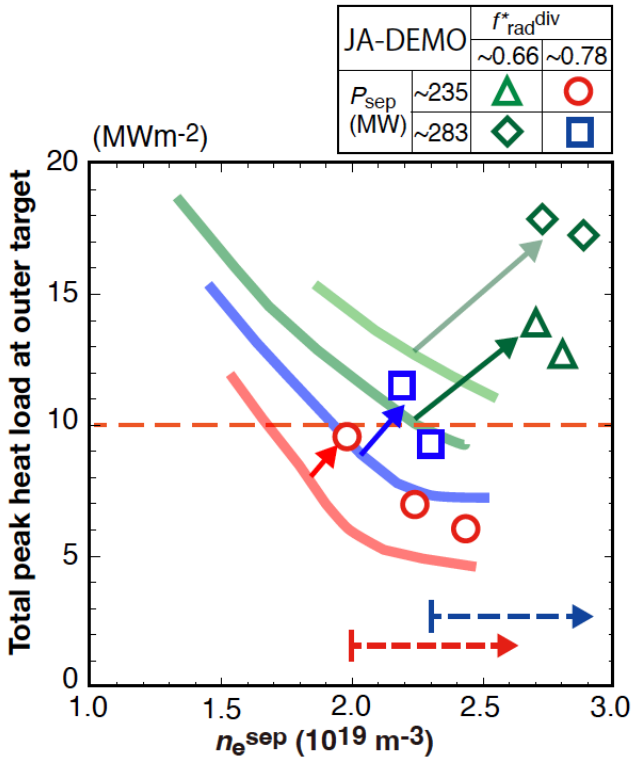

Figure 12 (2 columns)

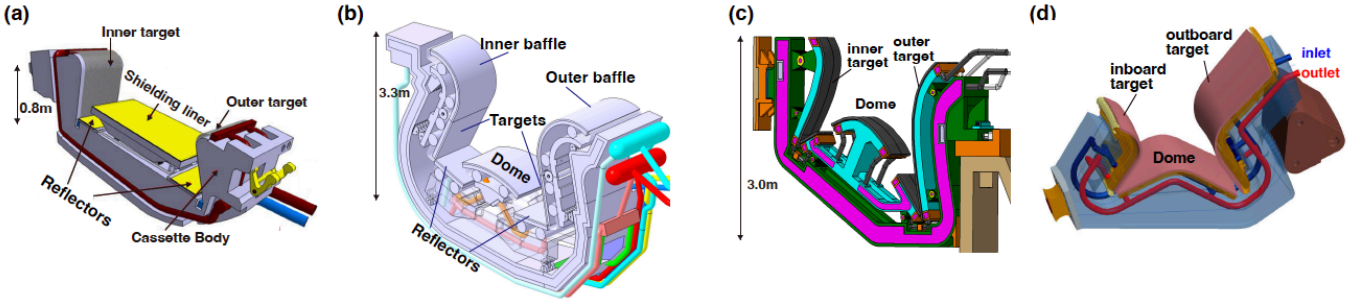

Figure 13 (1 column)

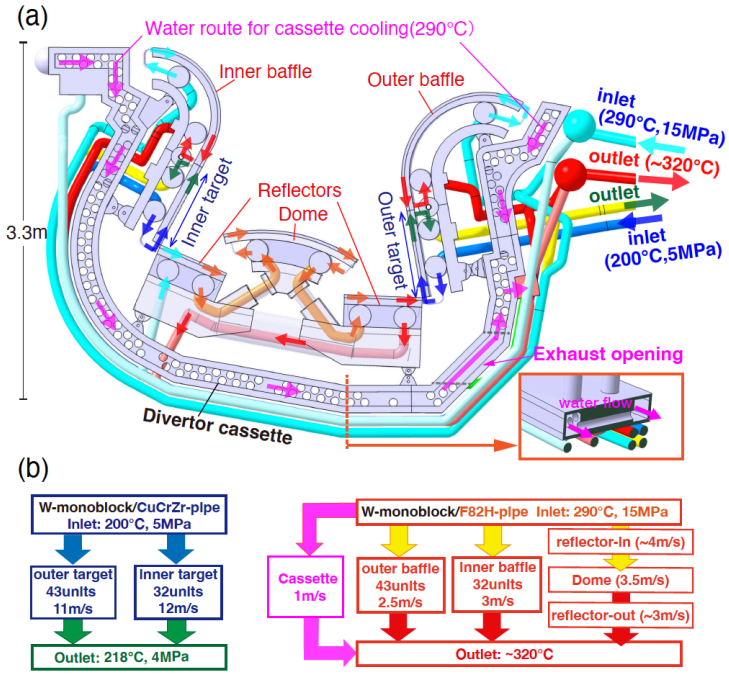

Figure 14 (1 column)

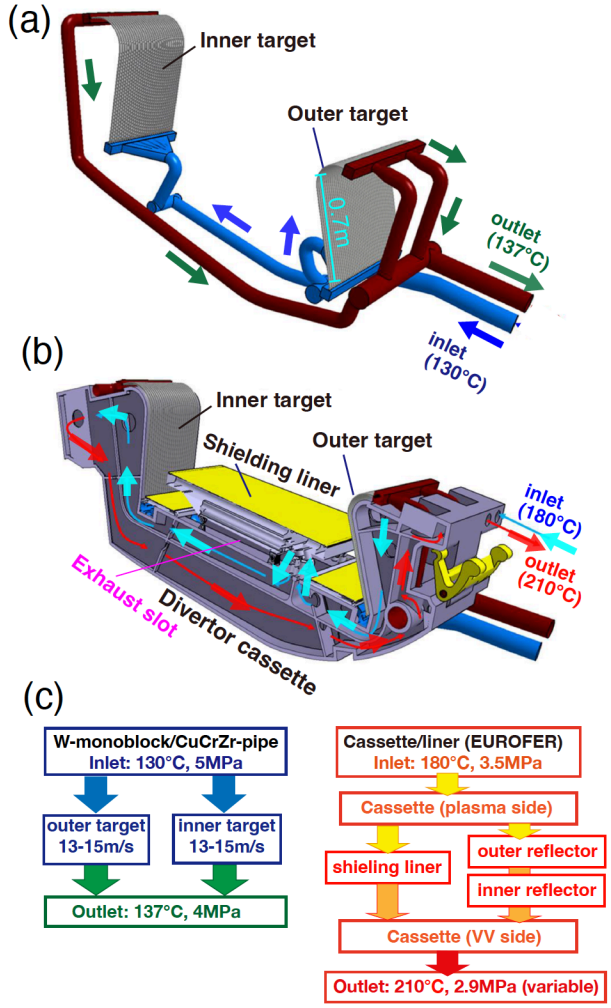

Figure 15(1 column)

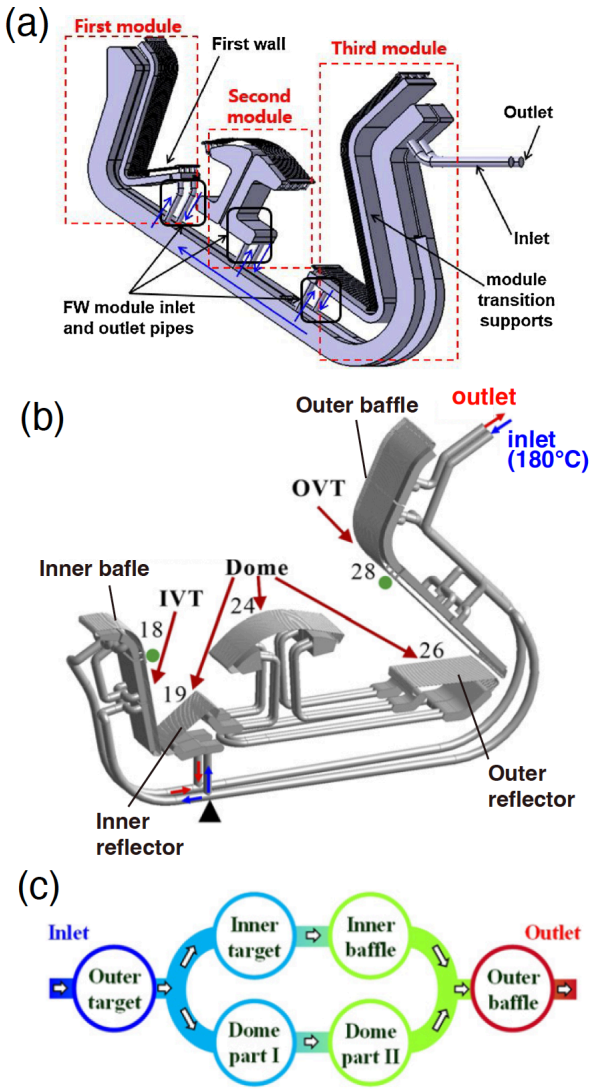

Figure 16(2 column)